ATMOSPHERIC COMPUTATIONS TO ASSESS ACIDIFICATION IN EUROPE: WORK IN PROGRESS

Extended abstracts from an International Technical Meeting cosponsored by IIASA and IMGW, Warsaw, 4–5 September 1980

Editors
Joseph Alcamo* and Jerzy Bartnicki**
* *International Institute for Applied Systems Analysis, Austria*
** *Institute for Meteorology and Water Management, Poland*

RR-86-5
November 1986

INTERNATIONAL INSTITUTE FOR APPLIED SYSTEMS ANALYSIS
Laxenburg, Austria

International Standard Book Number 3–7045–0078–x

Research Reports, which record research conducted at IIASA, are independently reviewed before publication. However, the views and opinions they express are not necessarily those of the Institute or the National Member Organizations that support it.

Cover design by Martin Schobel

Printed by Novographic, Vienna, Austria

SUMMARY

This Research Report contains extended summaries of papers presented at an international technical meeting held in Warsaw, September, 1985. The topics discussed include uncertainty analysis of long-range transport models, the current status of selected long-range transport models of particular relevance to policy analysis, and technical problems associated with the linkage of air pollution and ecological models.

FOREWORD

To investigate a transboundary problem, such as acidification of Europe's environment, there clearly needs to be good working relationships between scientists from all countries. A collaborative agreement between the Institute of Meteorology and Water Management (IMGW) in Warsaw and the International Institute for Applied Systems Analysis (IIASA) has helped build such relationships, to which Drs. Leen Hordijk and Jerzy Pruchnicki have made a valuable contribution as administrative coordinators. As part of this agreement IIASA and IMGW jointly sponsored a technical meeting on atmospheric computations in Warsaw, 4–5 September 1985, which brought together scientists from 11 different countries. This volume is a record of their discussions.

R.E. MUNN
Leader, Environment Program
International Institute for Applied Systems Analysis

CONTENTS

INTRODUCTION

Joseph Alcamo* and Jerzy Bartnicki**
* *International Institute for Applied Systems Analysis, Austria*
** *Institute for Meteorology and Water Management, Poland*

To understand acidification of the environment we must probe into a complicated system of materials cycling that covers vast time and space scales. Because of its large dimensions it is difficult to grasp the workings of this system by measurement and observation alone. For additional insight we use mathematical models, which synthesize and organize both empirical data and theoretical knowledge about the acidification system.

This Research Report examines some critical issues in the use of mathematical models, particularly those atmospheric models used in connection with the analysis of the acidification of Europe's environment. It is based on a meeting cosponsored by the International Institute for Applied Systems Analysis (IIASA) and the Institute for Meteorology and Water Management (IMGW) in Warsaw, 4–5 September 1985, and is a summary of meeting discussions, in the form of extended abstracts of the presentations. Contributions are arranged according to their order of presentation at the meeting and mostly describe work-in-progress with special emphasis on innovative methods. A follow-up meeting is planned for Spring, 1987, in which many of these scientists will present the results of the application of their methods.

This volume is organized according to the three topics of the meeting:

(1) Methods for estimating the uncertainty of long-range transport models. (Hereafter abbreviated as LRT models.)
(2) Status of long-range transport models in Europe relevant to decision making.
(3) Linkage between air quality and ecological models.

In Part One, on uncertainty analysis, a series of authors (Alcamo, Bartnicki, den Tonkelaar, Posch, and Pitovranov) report on work connected with the IIASA Acid Rain Project's investigation of uncertainty in long-range transport models. This analysis initially focused on the model developed at the Meteorological Synthesizing Center-West of EMEP (hereafter referred to as EMEP-West). Topics include a general framework for uncertainty analysis of LRT models, a method to evaluate parameter and other model uncertainties using Monte Carlo simulation, and methods to take into account the effect of

interannual meteorologic variability, as well as climate change, on computed sulfur deposition. In addition, Joffre and Nordlund present chapters on uncertainty in LRT models resulting from the so-called "local deposition" parameter and pollutant dry deposition over the sea.

In Part Two, on the status of LRT modeling in Europe, Eliassen *et al.* and Mikhailova report, respectively, on the status of long-range transport models of the EMEP-West and EMEP-East (Meteorological Synthesizing Center-East of EMEP). Berkowicz and Zlatev present results of model experiments using a nonlinear LRT NO_x model, which were conducted to determine if "built-in" model nonlinearities affect the linearity of a computed source–receptor relationship. On the same topic, van Aalst explains a simplified chemical scheme for computing regional scale ozone levels, which is of potential relevance to LRT models.

Part Three concerns linkages between atmospheric and ecological models where "atmospheric" and "ecological" are broadly defined. "Atmospheric models" in this context are models that describe air pollutant concentrations or flux, and ecological models include models that describe the interaction between nonliving and living elements of soil, water, and forest ecosystems. Gravenhorst and Mäkelä discuss these linkages from the atmospheric scientist and forest ecologist perspectives, respectively. Following them, Kämäri presents parameterizations of key connections between atmospheric inputs and lake and soil acidification. In the concluding chapter of Part Three, van Aalst presents some empirical data and a theoretical model of the vertical profile of SO_2. This profile is, of course, very relevant to the linkage between atmospheric models and ecological models, since atmospheric models often assume complete SO_2 mixing in the boundary layer, whereas ecological models are usually concerned with vertical scales much smaller than the boundary layer height.

Taken together, the three parts of this volume raise some of the most important issues involved in the use of mathematical tools to study the long-range transport of air pollutants.

PART ONE: UNCERTAINTY OF LONG-RANGE TRANSPORT MODELS

Summary of Paper Presented at the International Technical Meeting on *Atmospheric Computations for Assessment of Acidification in Europe: Work in Progress*. Cosponsored by IIASA and IMGW. Warsaw, 4–5 September 1985.

1. A FRAMEWORK FOR ASSESSING ATMOSPHERIC MODEL UNCERTAINTY

Joseph Alcamo
International Institute for Applied Systems Analysis, Austria

Long-range transport models have an important role in the study of regional and interregional air pollution problems (see, for example, OECD, 1979; US National Research Council, 1982). Naturally, with this important role comes the question: How credible are these models? An important aspect of this uncertainty is, ***what is the uncertainty of model results when they are used to evaluate future pollution control strategies***? In this sense ***model uncertainty*** is the departure of model calculations from current or future "true values". This paper presents a framework for the comprehensive analysis of environmental model uncertainty, specifically as it is applied to the so-called EMEP model of long-range atmospheric transport of sulfur in Europe (Eliassen and Saltbones, 1982) [1].

1.1. SENSITIVITY ANALYSIS AND DATA TESTING

There are two major reasons why conventional sensitivity analysis has an important, yet limited, role in uncertainty analysis. First, it is difficult to assess the sensitivity of model calculations to two or more variables simultaneously. Second, sensitivity analysis normally focuses on extreme values of variables, which provides insight for model development, but is less helpful in assessing the likely departure of model calculations from true values. Data testing, i.e., comparing model output against observations, is also important yet insufficient for uncertainty analysis because:

(1) Measurements are often incorrect.
(2) Model output is not necessarily observable in aggregated systems.
(3) Certain relationships may not be easily observable, e.g., the long-term relationship between pollutant emissions in a country and pollutant deposition in an area remote from these emissions.
(4) Agreement of model output with data does not settle the question of uncertainty when the model is used for forecasting purposes.

(5) Sometimes model parameters can be "artificially-tuned" such that model output very closely agrees with observations.
(6) It is often difficult to assemble data for a comprehensive range of environmental conditions.

1.2. PROPOSED FRAMEWORK

A proposed comprehensive approach to environmental model uncertainty analysis, which incorporates data testing and sensitivity analysis, is described in the following paragraphs.

1.2.1. Problem Formulation

Despite the trivial nature of this step it is surprising how often investigators discuss uncertainty of a model without specifying the time and space scales of interest. The degree to which uncertainty can vary depending on spatial–temporal scales is illustrated in *Figure 1.1*, taken from a study of uncertainty in forecasting sulfur deposition due to interannual variation of precipitation and wind patterns (Alcamo and Posch, 1986). For the EMEP model, the spatial temporal scale of interest is given by

$$d_{ijk} = S_i \, a_{ijk}$$

where d_{ijk} (g S m^{-2} yr^{-1}) is the total sulfur deposition at grid location (j,k) due to country i during one year; S_i (t S yr^{-1}) is the total annual sulfur emission from country i; and a_{ijk} is the element of unit source–receptor matrix.

1.2.2. Inventory of Uncertainty

To assist in identifying and classifying sources of uncertainty for further analysis, we propose the following taxonomy:

(1) *Model structure* – uncertainty due to the particular collection of model variables in a model and how they are related.
(2) *Parameters* – uncertainty due to coefficients that are constant in time or space.
(3) *Forcing functions* – variables that inherently change with time and space.
(4) *Initial state* – uncertainty due to boundary and initial conditions.
(5) *Model operation* – uncertainty due to solution techniques of model equations, and preprocessing and postprocessing of model information.

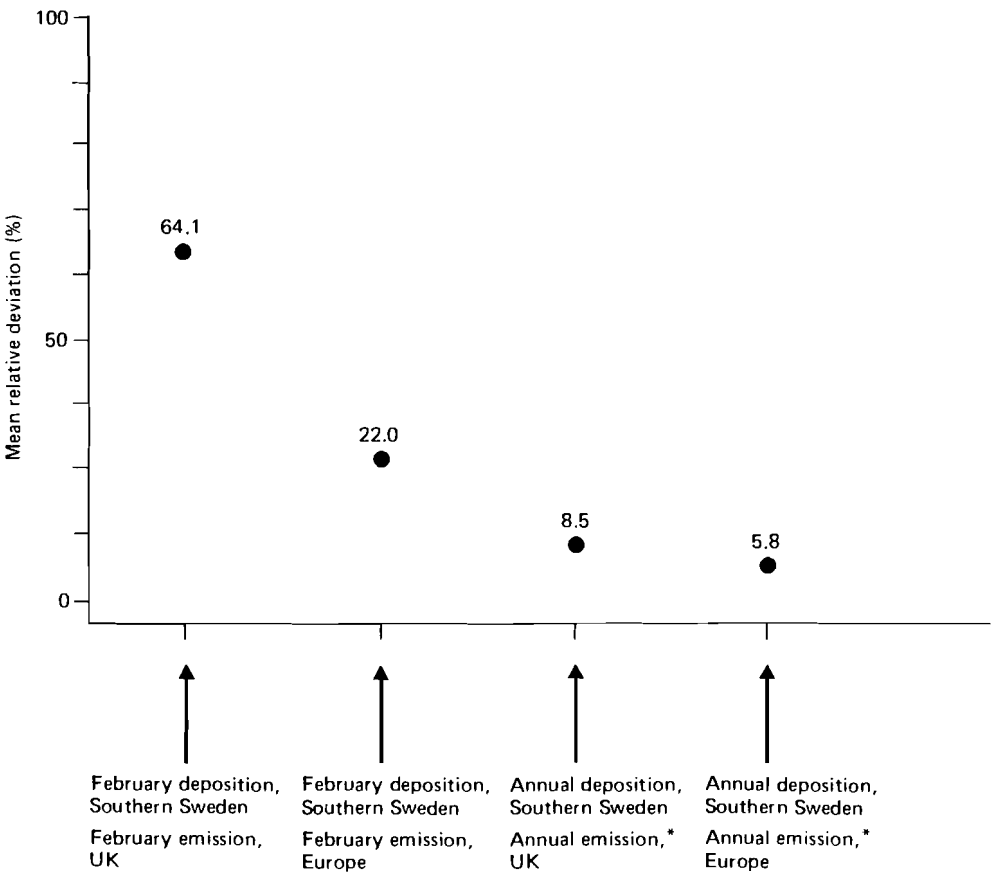

FIGURE 1.1. Variation in computed sulfur deposition due to interannual variability of meteorological inputs for different time–space scales of source–receptors (* = year 2010 reference scenario).

A further distinction is made between *diagnostic* and *prognostic* uncertainty, in which *diagnostic* uncertainty concerns model use to simulate past or present conditions and *prognostic* uncertainty obviously arises when the model is used to make forecasts. For illustrative purposes, we present in *Table 1.1* a preliminary application of this taxonomy to the EMEP model.

1.2.3. Screening and Ranking of Uncertainty

The goal of this step is to reduce the number of sources of uncertainty that need to be quantitatively evaluated in the next step. This is accomplished through conventional sensitivity analysis or qualitative judgment and need not have the identical time–space scales specified in step number one.

TABLE 1.1. Model uncertainty taxonomy with EMEP-West examples.[a]

	Diagnostic (past/current)	*Prognostic (forecasting)*
Model structure	Linearity	Linearity
Parameters	Parameter estimation errors	Parameter estimation errors
Forcing functions	Geographic distribution emissions	Future emissions
	Uncertain meteorologic inputs	Interannual meteorologic variability
Initial state	Boundary estimation errors	Future boundary conditions
Model operation	Trajectory estimation errors	Trajectory estimation errors

[a] This table is *not* an exhaustive inventory of possible model uncertainties. Examples are presented for illustration only.

1.2.4. Evaluation of Uncertainty

The sources of uncertainty that remain after step three can be evaluated by a number of different quantitative techniques. *Table 1.2* lists some approaches being taken in the IIASA Acid Rain Project to evaluate the EMEP model. Two of these approaches are presented in other papers of this Research Report (Alcamo and Posch, 1986; Bartnicki and Alcamo, 1986).

TABLE 1.2. Examples of techniques used to evaluate EMEP model uncertainty.

Type of uncertainty	*Technique*
Model structure	Model comparisons
Forcing functions, parameters, and initial state (estimation and approximation errors)	Monte Carlo analysis
Forcing functions (interannual meteorological variability)	Matrix analysis Statistical analysis of "Grosswetterlagen"
Forcing functions (climate change)	Historical data correlation

1.2.5. Application to Decision Making

One example of how to apply uncertainty information to decision making is illustrated by the RAINS model output shown in *Figures 1.2* and *1.3*. The RAINS model links a source–receptor matrix from EMEP with other submodels that describe the production of sulfur emissions and how the terrestrial and aquatic environment is affected by sulfur deposition (see, for example, Alcamo *et al.*, 1985; Hordijk, 1985). The model user can select a number of *indicators* to assess the impact of a user-specified pollution control program. One such indicator, featured in *Figures 1.2* and *1.3*, is sulfur deposition. In these figures we have also indicated the influence of a ± 13% confidence interval in forecasted sulfur deposition [2]. It is interesting that despite an assumed constant confidence interval, the importance of uncertainty significantly varies spatially (*Figure 1.2*) and temporally (*Figure 1.3*). This is due to background deposition and the spatial–temporal pattern of sulfur emissions interacting in a complicated manner.

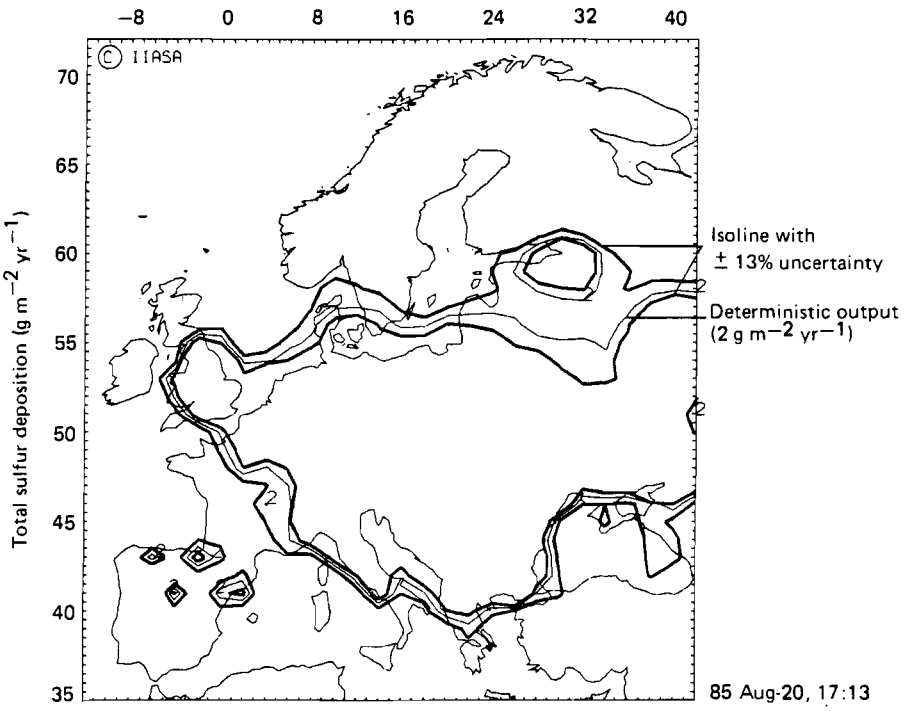

FIGURE 1.2. Computed sulfur deposition with ± 13% confidence interval (reference scenario, year 2010).

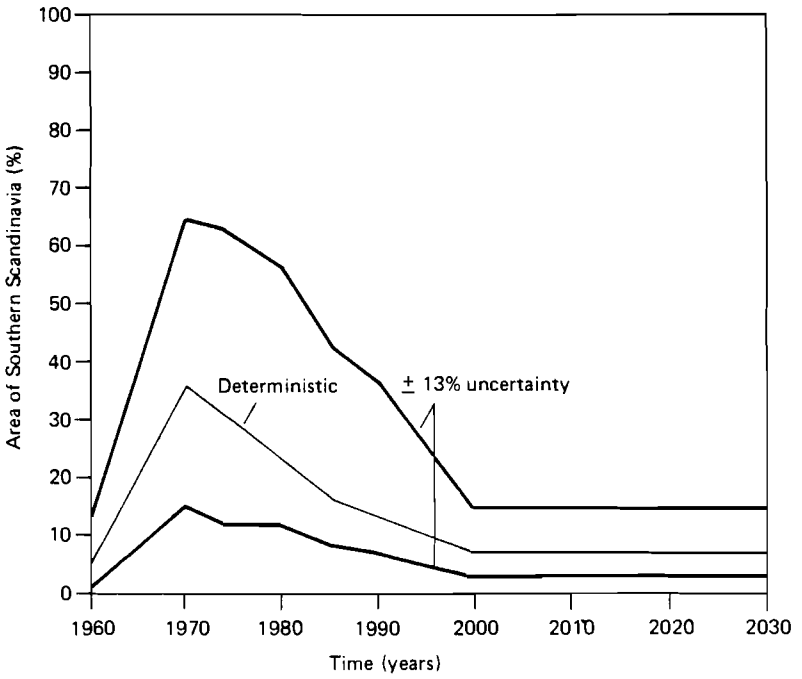

FIGURE 1.3. Computed area covered by > 2.0 g m^{-2} yr^{-1} sulfur deposition with ± 13% confidence interval for Southern Scandinavia (reference scenario).

1.3. CONCLUSIONS

(1) The framework briefly described in this paper, and in greater detail in Alcamo and Bartnicki (1985), can be a starting point for a comprehensive assessment of atmospheric model uncertainty.

(2) Examples presented in this paper suggest that the importance of uncertainty in model calculations can vary tremendously, depending on the temporal and spatial scales of interest. Moreover, with respect to sulfur deposition, a constant confidence interval can create greatly varying spatial and temporal patterns of model uncertainty.

NOTES

[1] A more detailed treatment of the ideas presented in this paper can be found in Alcamo and Bartnicki (1985).

[2] In another paper (Alcamo and Posch, 1986), we estimate that the *average* uncertainty in an EMEP grid element due to interannual variations of meteorology is approximately 13%.

REFERENCES

Alcamo, J. and Posch, M. (1986), Effect of interannual meteorologic variability on computed sulfur deposition in Europe, Chapter 6, this volume.

Alcamo, J. and Bartnicki, J. (1985), *An Approach to Uncertainty of a Long Range Transport Model*, Working Paper WP-85-88 (International Institute for Applied Systems Analysis, Laxenburg, Austria).

Alcamo, J., Hordijk, L., Kämäri, J., Kauppi, P., Posch, M., and Runca, E. (1985), Integrated analysis of acidification in Europe, *J. Environ. Manage.*, **21**, 47–61.

Bartnicki, J. and Alcamo, J. (1986), Assessing atmospheric model uncertainty by using Monte Carlo analysis, Chapter 2, this volume.

Eliassen, A. and Saltbones, J. (1983), Modeling of long-range transport of sulfur over Europe: a two-year model run and some model experiments, *Atmos. Environ.*, **17**(8), 1457–1473.

Hordijk, L. (1985), A model for evaluation of acid deposition in Europe, in A. Sydow (Ed), *Systems Analysis and Simulation 1985, Volume II: Applications*, pp 30–39 (Akademie-Verlag, Berlin).

OECD (1979), *Long Range Transport of Air Pollutants* (OECD, Paris).

US National Research Council (1981), *Atmosphere–Biosphere Interactions: Toward a Better Understanding of the Ecological Consequences of Fossil Fuel Combustion* (National Academy Press, Washington, DC).

Summary of Paper Presented at the International Technical Meeting on *Atmospheric Computations for Assessment of Acidification in Europe: Work in Progress*. Cosponsored by IIASA and IMGW. Warsaw, 4–5 September 1985.

2. ASSESSING ATMOSPHERIC MODEL UNCERTAINTY BY USING MONTE CARLO SIMULATION

Jerzy Bartnicki* and Joseph Alcamo**
* *Institute for Meteorology and Water Management, Poland*
** *International Institute for Applied Systems Analysis, Austria*

In another chapter of this volume we propose a taxonomy for classifying sources of uncertainty in environmental models (Alcamo, 1986). In this summary we briefly describe the use of Monte Carlo Simulation (MCS) to quantitatively evaluate the importance of three of these uncertainty classes – parameters, forcing functions, and initial state – in the EMEP model [1].

2.1. PROCEDURE

In this application we use MCS to obtain the frequency distribution of output variables in the EMEP model. The output variables include SO_2 air concentration, SO_4^{2-} air concentration, and wet, dry, and total sulfur deposition. For illustration, we describe how MCS is used to obtain the frequency distribution of one of these state variables, SO_2 air concentration. We represent SO_2 air concentration by c_t in the following equation:

$$c_t = g[x, t, \alpha_1, \ldots, \alpha_m, \beta_1, \ldots, \beta_n, c_t(0)] \tag{2.1}$$

where c_t is a function of space (x), time (t), forcing functions (α_1 to α_m), parameters (β_1 to β_n), and the boundary and initial conditions of c_t [$c_t(0)$].

Using random numbers ν, $\mu \in [0,1]$ we "sample" the cumulative frequency distributions $F(\cdot)$ [2] of each α and β, to obtain α^i and β^i such that $F(\alpha^i) = \nu$ and $F(\beta^i) = \mu$.

Each α^i and β^i is used to compute c_t by equation (2.1). An individual computation of c_t is called a ***realization*** of c_t. We repeat this sampling and computation procedure N times until a statistically significant sample of each

α and β is drawn. We then compute the frequency and cumulative frequency distributions of c_t from the ensemble of realizations of c_t:

$$\left\{c_{t,i}\right\}_{i=1}^{N} \rightarrow f(c_t) \text{ or } F(c_t)$$

The frequency distribution $f(c_t)$ indicates the uncertainty of SO_2 air concentration due to the uncertainty reflected in $F(\alpha_1),\ldots, F(\alpha_m)$ and $F(\beta_1),\ldots, F(\beta_n)$.

2.2. SELECTING INPUT FREQUENCY DISTRIBUTIONS

A critical exercise in this method is to intelligently select the frequency or cumulative frequency distributions of parameters and forcing functions. Interpretation of these frequency distributions becomes a key issue because through their selection we express our *a priori* uncertainty about these variables. For example, what time and space scales should the distributions reflect? What kind of information should we use to select a distribution if the variable is too "lumped" to be observed in nature? Does the prescription of frequency distributions for a particular parameter imply acceptance of the model structure? These and other questions are being addressed in the course of the IIASA uncertainty analysis. However, in order to illustrate the method we have made some *ad hoc* assumptions about the frequency distributions of four of the parameters in the EMEP model. For example, we have assumed that they represent the frequency of occurrence of particular annual and European-average values. Moreover, we have assumed that they are triangular-shaped, with EMEP parameter values as the median and extremes based on the literature and expert opinion. As a result we have selected the distributions shown in *Figure 2.1*.

2.3. PRELIMINARY RESULTS

We examine how EMEP state variables are affected by the assumed frequency distributions of the four parameters in a case study of UK sulfur emissions and Southern Sweden sulfur deposition. This is only the first of five case studies. The source–receptor combinations that have not yet been analyzed are: Netherlands–Northern Denmark, Czechoslovakia–Northern GDR, GDR–Eastern Austria, Poland–Central Hungary. These combinations were selected to cover a wide range of geographic and meteorologic conditions.

Figure 2.2 presents the resulting frequency distribution of SO_2 (air). This figure reflects the uncertainty in the computed annual average SO_2 air concentration in an EMEP grid element in Southern Sweden (resulting from UK emissions) due to the uncertainty of v_d, h, k_t, and k_w. The coefficients of

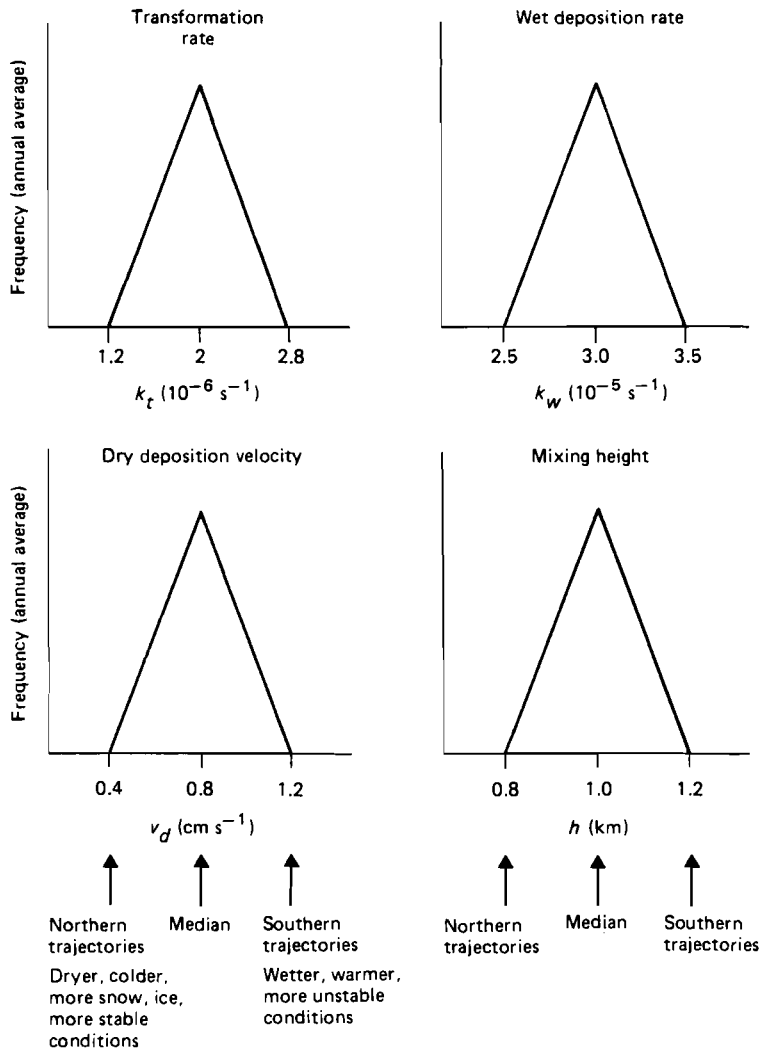

FIGURE 2.1. Frequency distributions k_t, k_w, v_d, and h.

variation (c.v. = $\sigma/\bar{x}$) of computed SO_2 (air), SO_4^{2-} (air), dry sulfur deposition, wet sulfur deposition, and total sulfur deposition are reported in *Table 2.1*. Note that the largest c.v. occurs for SO_2 air concentration (27%) and the smallest for total sulfur deposition (9%). This reflects the integrative nature of sulfur deposition in the EMEP model. For all forms of deposition the c.v. is rather small (around 10%) suggesting that the uncertainty in computed deposition due to uncertainty in these four parameters is rather small. But this conclusion depends on the *a priori* acceptance of the model structure and

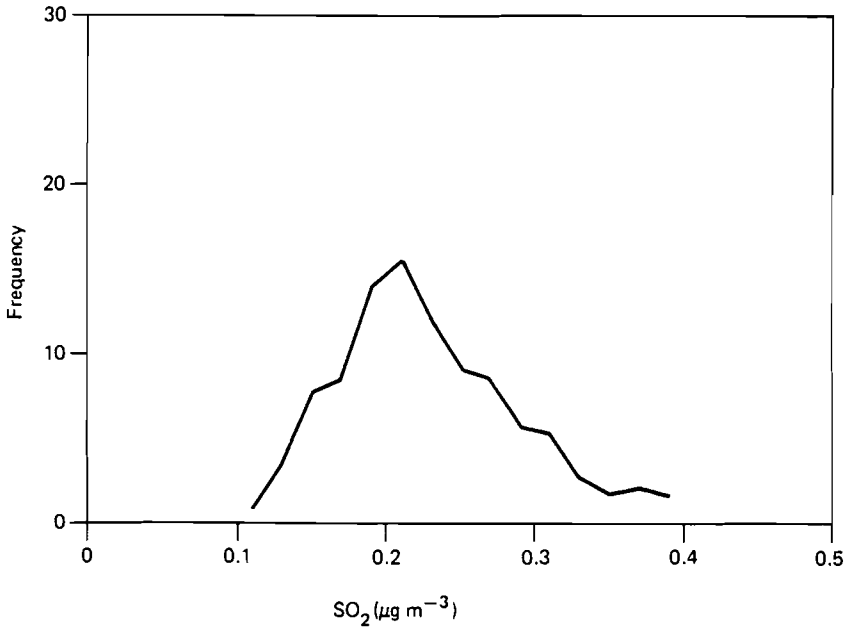

FIGURE 2.2. Computed frequency distribution of annual average SO_2 (air).

TABLE 2.1. Results from Monte Carlo simulations of EMEP parameter uncertainty: influence of simultaneous uncertainty of four parameters (v_d, h, k_t, k_w) on EMEP state variables.

State variables	*Coefficient of variation* (%)
SO_2 (air)	27
SO_4^{2-} (air)	14
Dry sulfur deposition	8
Wet sulfur deposition	11
Total sulfur deposition	9

confidence that the uncertainty of these parameters is reflected in the frequency distributions of *Figure 2.1*. Also, this method has so far been applied only to the UK–Southern Sweden case.

Table 2.2 presents the c.v. for SO_2 air concentration and total sulfur deposition as it is affected by the uncertainty of each of the four parameters individually. Note that v_d has the largest effect on uncertainty of SO_2 air concentration (c.v. = 23%), yet a small effect on total sulfur deposition (c.v. = 2%). An examination of the EMEP equations can explain this compensation, though the question remains as to whether nature behaves in the same manner.

TABLE 2.2. Results from Monte Carlo simulations of EMEP parameter uncertainty: influence of individual parameter uncertainty on EMEP state variables.

Parameter varied	*Coefficient of variation* (%)	
	SO_2 *(air)*	*Total sulfur deposition*
v_d	23	2
h	9	4
k_t	4	6
k_w	4	2
v_d, h, k_t, k_w	27	9

2.4. FURTHER RESEARCH

The preceding summary briefly outlines the research underway at IIASA in using MCS to examine EMEP model uncertainty. Some next steps in this research will include:

(1) Examining uncertainty due to a complete set of EMEP parameters, forcing functions, and initial states and for at least five source–receptor combinations.
(2) Comparing results using triangular, rectangular, and other frequency distribution types.
(3) Encoding opinion of several different atmospheric experts into the frequency distributions of the parameters, functions, and so on, by using a fixed protocol. Examining differences in forecasted state variables due to these different sets of input frequency distributions.
(4) Accounting for the co-variance of parameters.
(5) Using Bayesian analysis to combine data with *a priori* estimates of the frequency distributions of the parameters, functions, and so on.

ACKNOWLEDGMENT

W. Schöpp of the IIASA Acid Rain Project developed the computer program used to perform the calculations reported in this summary.

NOTES

[1] The so-called EMEP model is described in Eliassen and Saltbones (1983).
[2] $F(\cdot)$ is, in turn, commonly derived from the frequency distribution $f(\cdot)$.

REFERENCES

Alcamo, J. (1986), A framework for assessing atmospheric model uncertainty, Chapter 1, this volume.

Eliassen, A. and Saltbones, J. (1983), Modeling of long-range transport of sulfur over Europe: a two-year model run and some model experiments, *Atmos. Environ.*, **17**(8), 1457–1473.

Summary of Paper Presented at the International Technical Meeting on *Atmospheric Computations for Assessment of Acidification in Europe: Work in Progress*. Cosponsored by IIASA and IMGW. Warsaw, 4–5 September 1985.

3. DYNAMICAL AND AERODYNAMICAL FACTORS AFFECTING DRY DEPOSITION AND CONCENTRATION OF TRACE GASES OVER THE SEA

Sylvain Joffre
Finnish Meteorological Institute, Finland

3.1. INTRODUCTION

In most long-range transport (LRT) models, the deposition rate at the surface and the height of the mixing layer are taken as model constants implied from scarce and uncertain observations. When dealing with long-term statistical studies, there are some justifications for using these constant parameters to describe very complicated and fluctuating processes. On the other hand, if one is interested in specific LRT episodes, then dramatic errors can obviously be observed. However, even in the case of statistical studies like those performed in the framework of the EMEP, the study area is so large with very different types of surfaces and different diurnal or varying seasonal conditions (e.g., overland and oversea conditions), that repeated trajectory computations with average-condition parameters in the model much different from the characteristic ones can lead to systematic differences in the long-term results.

3.2. DRY DEPOSITION VELOCITY IN THE FRAMEWORK OF SURFACE LAYER SCALING

The most current approximation for the surface flux $\overline{w'X'}$ of a constituent of concentration X is

$$-\overline{w'X'} = v_d X(z_r) \tag{3.1}$$

where v_d is the deposition velocity and z_r the reference height. For the transfer to water surfaces, the difficulty lies in the fact that surface characteristics are a function of the flow with interaction processes, like wave

generation, spray formation, and mixing in the water. The air in contact with the aquatic surface is saturated with water vapor, enhancing the possibility of chemical reactions and diffusiophoresis, and the surface may be a strong source, rather than a sink, for some particles and gases. Since it is not possible for the flux of a gaseous pollutant to the surface to exceed the limits imposed by the diffusive capability of the atmospheric surface layer, aerodynamic resistance is clearly a potentially limiting factor in deposition and uptake.

By analogy with the transfer of momentum, heat, or water vapor, we can write for the vertical distribution of a trace constituent in the surface layer

$$\bar{X}(z_r) - X_0 = \frac{-\overline{w'X'}}{k u_* a_x}\left\{\ln(z_r / z_{0x}) - \psi(z_r / L_*)\right\} \tag{3.2}$$

where X_0 is the concentration at the height z_{0x} (constituent roughness length or capture length), u_* the friction velocity, k the von Karmen constant, a_x^{-1} the eddy Schmidt number, and ψ a function describing thermal stability effects and dependent only on the parameter z/L_*, where $L_* = -u_*^3 T / gkQ_0$ and $Q_0 = \left[\overline{w'T'_v}\right]$ is the heat flux. Without much loss of generality we can assume that $X_0 = X_s$, the actual surface value. Moreover, taking the case of sulfur dioxide we have no surface resistance and $X_s = 0$. Identifying equations (3.1) and (3.2) yields

$$v_d = \frac{k u_* a_x}{\ln(z_r / z_{0x}) - \psi} \tag{3.3}$$

We see from equation (3.3) that the deposition velocity is a function of wind speed (through u_*), surface roughness for the constituent, and thermal stability. This is the basic equation that describes the aerodynamic character of the deposition velocity and we shall examine here how variable meteorological parameters affect v_d.

3.3. THE CAPTURE LENGTH FOR DIFFUSED QUANTITIES

We propose to use the expressions derived by Brutsaert (1975) for water vapor roughness, z_{0v} (and assuming $z_{0v} = z_{0x}$), which have been tested against experimental data and have the advantage of depending on flow conditions. For rough conditions (the majority of cases with $Re_* \geq 2$),

$$z_{0v} = 7.4\, z_0 \exp\left\{-7.3k\, Re_*^{0.25}\, Sc^{0.5} a_v\right\} \tag{3.4}$$

where $Re_*(= u_* z_0 / \nu)$ is the Reynolds number, $Sc(= \nu / D_w)$ the Schmidt number, z_0 the roughness length, ν the kinematic viscosity, and D_w the diffusivity of water vapor in air. The large variations of z_{ov} with wind speed are illustrated in *Figure 3.1*. On the other hand, z_{ov} does not have the same behavior as z_0.

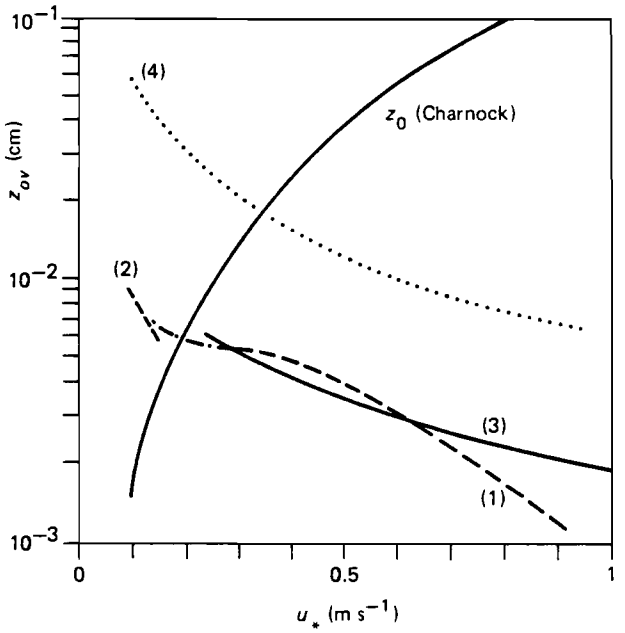

FIGURE 3.1. Dependence of the water vapor roughness z_{ov} on friction velocity u_* according to different models. Brutsaert's (1975) model [equation (3.4)] with $z_0 = 0.0144\, u_*^2/g$ [dashed curve (1)], with $z_0 = 0.0132$ cm [full curve (3)], and for smooth conditions [dashed curve (2)]. The relationship $z_{ov} = D_w / k u_*$ is shown as the dotted curve (4). The dotted–dashed curve is a simple interpolation between the smooth and rough regimes of Brutsaert's model.

The effect of stability on the deposition velocity [using curve (4) in *Figure 3.1*] is illustrated in *Figure 3.2* following Hicks and Liss (1976). It appears that v_d can vary by a factor of 2 or 3. Consequently, it would seem important to express properly the dependence of dry deposition velocity on wind speed and thermal stability. A simple practical parameterization is discussed later.

3.4. EFFECTS OF DRY DEPOSITION VARIATIONS ON PLUME DEPLETION

Assuming neutral thermal conditions, the airborne concentration depletion for an overwater, dry episode (no precipitation scavenging, no source) can be expressed as

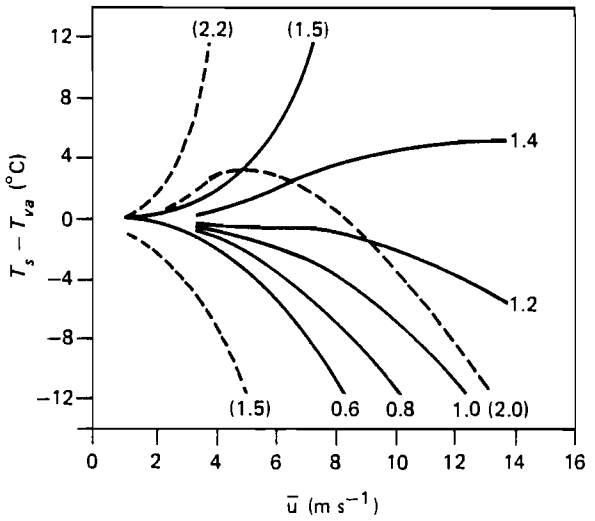

FIGURE 3.2. Isopleths of the ratio $(v_d / \bar{u}) \times 10^3$ relevant to observations made at 10 m height (solid curves) and 1 m height (broken curves) over open ocean. $T_s - T_{va}$ is the virtual potential temperature difference between the surface and the height of observation and $\bar{u}$ is the wind speed at the same level (from Hicks and Liss, 1976).

$$d\bar{X}/dt = -v_d\bar{X}/h \tag{3.5}$$

where h is the mixing height. Equation (3.5) implies an exponential decrease of $\bar{X}$. Note that this expression implies a direct coupling between surface processes and the dynamics of the whole boundary layer expressed in h.

The EMEP model assumes $v_d = 0.8$ cm s^{-1} for SO_2 and $h = 1000$ m (mean residence time of 35 hours). Using equation (3.3) for v_d and equation (3.4) for z_{ox}, we can apply equation (3.5) to a strong overwater transport episode ($u_* = 0.55$ m s^{-1} and $h = 800$ m) implying a residence time of 10 hours and a mean transport of 600 km before deposition [curve (1) in *Figure 3.3*]. These values are in good agreement with the values deduced by Prahm *et al.* (1976). Considering an episode under stable stratification conditions with weak winds ($u_* = 0.1$ m s^{-1} and $h = 200$ m) we obtain curve (2) in *Figure 3.3*. These two curves are very distinct from the EMEP dry depletion curve. Finally, we compute v_d from equation (3.3) for a rough continental surface with $z_0 = 0.5$ m and moderate wind conditions ($u_* = 0.35$ m s^{-1}); after solving equation (3.5) with $h = 1000$ m we obtain curve (3) in *Figure 3.3*, which is very similar to the EMEP curve, so that the latter corresponds rather to overland situations. *Table 3.1* gives some overwater values of v_d for SO_2 taken from the literature.

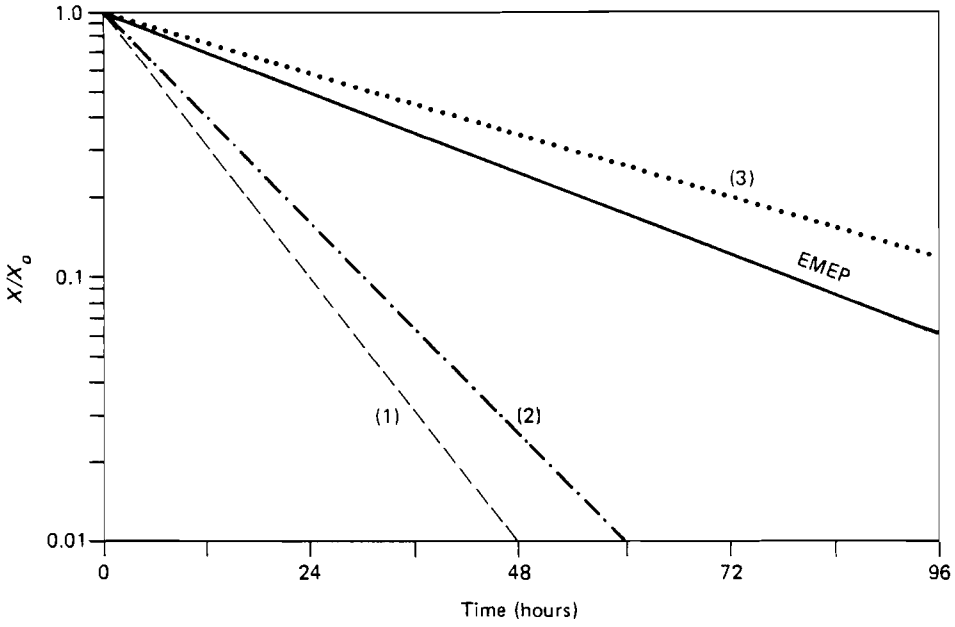

FIGURE 3.3. Illustration of the depletion law $X/X_0 = \exp(-v_d/h)$ with travel time according to different dry deposition models. EMEP model, $v_d = 0.8$ cm s^{-1}, $h = 1$ km; curve (1), overwater conditions with strong wind, $u_* = 0.55$ m s^{-1}, $h = 0.88$ km; curve (2), stable overwater conditions, $u_* = 0.1$ m s^{-1}, $h = 0.2$ km; curve (3), rough overland case with $u_* = 0.35$ m s^{-1}, $z_0 = 0.5$ m, and $h = 1$ km.

3.5. MIXING HEIGHT VARIATIONS OVER THE SEA

In the above example calculations we used different values of the mixing height h, while the EMEP model uses a constant h. *Figures 3.4* and *3.5* show some compiled data for h over sea areas as a function of surface virtual heat flux and surface wind speed, respectively. Note that h is mainly between 400 and 800 m for those data covering different seasons but mainly summer conditions. Higher values of h (1000–2000 m) are reached only under very strong wind conditions, $V_{10} > 15$ m s^{-1}, and/or especially large upward virtual heat fluxes ($H_{v0} > 80$ W m^{-2}), typical of fall or early winter conditions.

The effect of horizontal heterogeneity [i.e., $v_d = v_d(x,y)$ and $h = h(x,y)$] across a midlatitude cyclone on plume depletion is also discussed, showing that significant differences in plume depletion are observed over even short fetches.

TABLE 3.1. Observed values of v_d (cm s^{-1}) for SO_2 over water surface.

v_d	z (m)	*Comments*	*Sources*
0.7			Huser *et al.* (1978)
0.2		Calm	Spedding (1972)
1.4		Turbulent	
0.45			Liss and Slater (1974)
0.9	0.2		Owers and Powell (1974)
0.5	0.05		
4		Unstable	
2.2	2	Neutral	Whelpdale and Shaw (1974)
0.16		Stable	
0.46			Garland (1976)
2			Prahm *et al.* (1976)
0.41			Garland (1977)
0.5			Smith and Hunt (1978)
1.07 ± 1.05		average of the 13 values above	

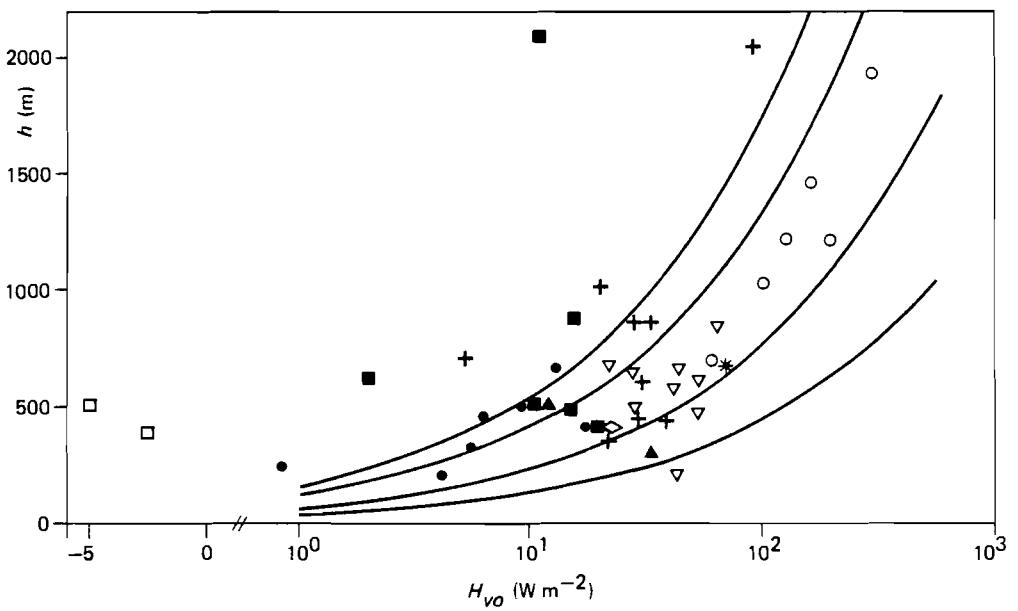

FIGURE 3.4. Empirical dependence of the mixing layer height h on surface virtual heat flux. The continuous curves are results of Tennekes' (1973) model $h = (2Q_{vo}t/\gamma)^{0.5}$ for different values of time t and the temperature vertical gradient γ above the mixing height; the symbols represent empirical data from various investigators (see Joffre, 1985).

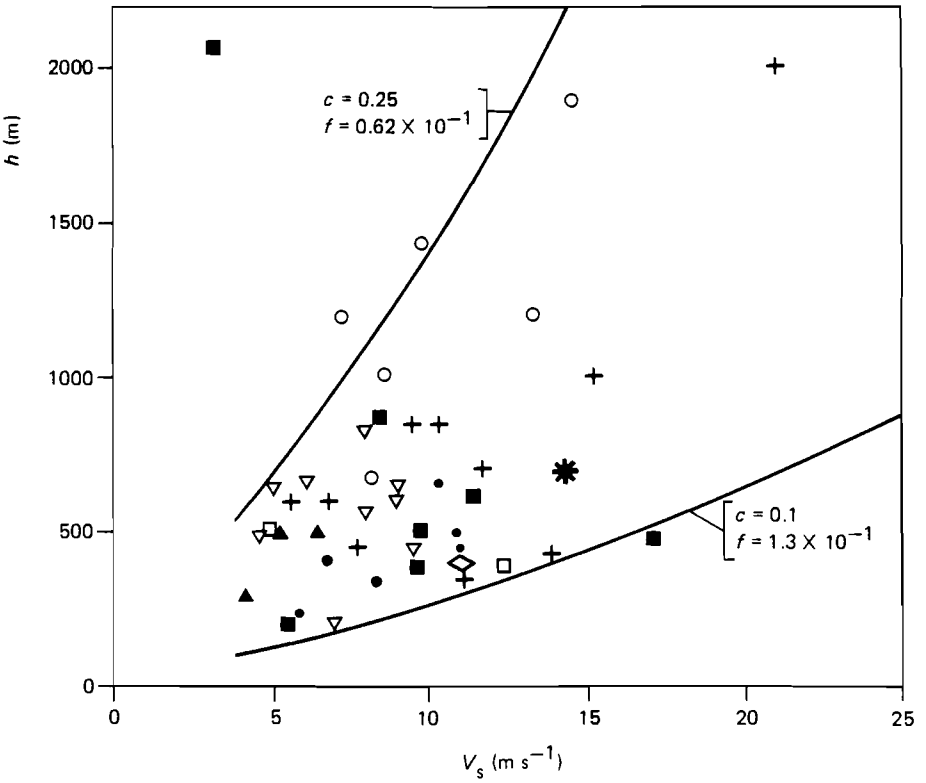

FIGURE 3.5. Scatter diagram for the dependence of the mixing layer height on surface wind velocity V_s. The continuous curves are for the neutral Ekman layer model $h = cu_*/f$ (from Joffre, 1985). Empirical data as in *Figure 3.4*.

3.6. CONCENTRATION PROFILES

In most models, a well-mixed structure is assumed with pollutant species having a vertically homogeneous distribution all through the mixing layer. In order to be more realistic, one can match this homogeneous distribution to the non-homogeneous profile [equation (3.2)] within the surface layer. However, fluxes at both the surface and the top of the mixing layer alter this ideal situation and non-zero vertical gradients can be observed within the bulk of the mixed layer. The decrease of specific humidity across the mixed layer under convective conditions (with temperature well-mixed) has been parameterized by André *et al.* (1979). Fairall and Larsen (1984) noted also the importance of entrainment fluxes for the aerosol distribution within the marine atmospheric boundary layer. Recently, Wyngaard (1984) presented a model for the concentration profiles of trace constituents within the mixing layer.

3.7. CONCLUDING REMARKS

This theoretical framework, in which dry deposition velocity depends on the characteristics of flow over well-developed wind waves, applies only to gases that have the main resistance to deposition in the gas phase and a high solubility or rapid aqueous-phase reaction rate (e.g., H_2O, SO_2, NH_3, NO_2, SO_3, HCl, HF). On the other hand, this model should be modified (see e.g., Slinn *et al.*, 1978; Fitzjarrald and Lenschow, 1983) for:

(1) Those gases not perfectly absorbed by the ocean with a flux back to the atmosphere.
(2) Those gases having resistance within the liquid phase.
(3) Those gasses having a short reaction time with turbulent transfer, maintaining the system in a state removed from chemical equilibrium (e.g., NO, NO_2, O_3).

More detailed data on concentration profiles are needed and especially accurate measurements of trace gas concentrations in seawater. As regards the variety of reference levels for the determination of v_d, a level of 4–5 m can also be recommended.

REFERENCES

André, J.C., Lacarrère, P., and Mahrt, L.J. (1979), Sur la distribution verticale de l'humidité dans une couche limite convective, *J. Rech. Atmos.*, **13**(2), 135–146.

Brutsaert, W. (1975), The roughness length for water vapor, sensible heat, and other scalars, *J. Atmos. Sci.*, **32**, 2028–2031.

Fairall, C.W. and Larsen, S.E. (1984), Dry deposition, surface production and dynamics of aerosols in the marine boundary layer, *Atmos. Environ.*, **18**(1), 69–77.

Fitzjarrald, D.R. and Lenschow, D.H. (1983), Mean concentration and flux profiles for chemically reactive species in the atmospheric surface layer, *Atmos. Environ.*, **17**(12), 2505–2512.

Garland, J. (1976), Dry deposition of SO_2 and other gases, *Proc. Symp. on Surface Exchange of Particulate and Gaseous Pollutants – 1974*, pp 212–217 (Richland, Washington).

Garland, J. (1977), The dry deposition of sulfur dioxide to land and water surfaces, *Proc. R. Soc.*, **A354**, 245–268.

Huser, R.B., Lodge, J.P., and Moore, D.J. (Eds) (1978), Sulfur in the atmosphere. Proc. Int. Symp. Dubrovnik, September 1977, *Atmos. Environ.*, **12**, 7–23.

Hicks, B.B. and Liss, P.S. (1976), Transfer of SO_2 and other reactive gases across the air–sea interface, *Tellus*, **28**(4), 348–354.

Joffre, S.M. (1985), *The Structure of the Marine Atmospheric Boundary Layer: A Review from the Point of View of Diffusivity, Transport and Deposition Processes*, Technical Report No. 29 (Finnish Meteorological Institute, Helsinki).

Liss, P.S. and Slater, P.G. (1974), Flux of gases across the air–sea interface, *Nature*, **247**, 181–184.

Owers, M.J. and Powell, A.W. (1974), Deposition velocity of sulfur dioxide on land and water surfaces using a S35 tracer method, *Atmos. Environ.*, **8**(1), 63–67.

Prahm, L.P., Torp, U., and Stern, R.M. (1976), Deposition and transformation rates of sulfur oxides during atmospheric transport over the Atlantic, *Tellus*, **28**(4), 355–372.

Slinn, W.G.N., Hasse, L., Hicks, B.B., Hogan, A.W., Lal, D., Liss, P.S., Munnich, K.O., Sehmel, G.A., and Vittori, O. (1978), Some aspects of the transfer of atmospheric trace constituents past the air–sea interface, *Atmos. Environ.*, **12**(11), 2055–2087.

Smith, F.B. and Hunt, R.D. (1978), Meteorological aspects of the transport of pollution over long distances, *Atmos. Environ.*, **12**, 461–477.

Spedding, D.J. (1972), Sulfur dioxide absorption by sea water, *Atmos. Environ.*, **6**, 583–586.

Tennekes, H. (1973), A model for the dynamics of the inversion above a convective boundary layer, *J. Atmos. Sci.*, **30**(4), 558–567.

Whelpdale, D.M. and Shaw, R.W. (1974), Sulfur dioxide removal by turbulent transfer over grass, snow and water surfaces, *Tellus*, **26**, 195–204.

Wyngaard, J.C. (1984), Toward convective boundary layer parameterization: a scalar transport module, *J. Atmos. Sci.*, **41**(12), 1959–1969.

Summary of Paper Presented at the International Technical Meeting on *Atmospheric Computations for Assessment of Acidification in Europe: Work in Progress*. Cosponsored by IIASA and IMGW. Warsaw, 4–5 September 1985.

4. LOCAL DEPOSITION OF SULFUR: A COMPARISON OF FINNISH ESTIMATES AND EMEP MODEL (EMEP-WEST) VALUES

Göran Nordlund
Finnish Meteorological Institute, Finland

4.1. INTRODUCTION

In 1984–1985 an investigation called "Sulfur Deposition due to Finnish Sources" was carried out at the Finnish Meteorological Institute. For this investigation, model calculations of dry and wet deposition caused by different types of sources and source areas were made. A combined Gaussian and *K*-theory model was used as the dispersion model, in which the horizontal diffusion of pollutants was estimated by solving the diffusion equation (as defined by Calder, 1961) numerically. The assumed horizontal transition distance varied according to stability from 250 m in stable conditions to 1500 m in unstable conditions.

4.2. LOCAL DEPOSITION

The long-range dispersion model used in the ECE–EMEP project applies a factor (α) for "additional" dry deposition within the initial grid element (Eliassen, 1968). This additional local deposition, which is needed in order to compensate for errors due to the assumption of immediate mixing within the mixing layer, represents most of the initial dry deposition within the grid of emission. An average value of 0.15 has been applied for α in the ECE–EMEP model for a grid size of 150 × 150 km.

The α value depends on the stability of the atmospheric boundary layer, wind speed ($\bar{u}$), and effective emission height, as well as on the grid size and the dry deposition velocity v_d. The α value of the ECE–EMEP model is based on estimates of α for different types of urban areas and for different effective emission heights during neutral stability conditions and on a value of 10^{-3} for $v_d / \bar{u}$ (OECD, 1979; Eliassen, 1968).

TABLE 4.1. Local sulfur deposition factors (listed according to effective release height; deposition amount is given as percent of release) within a distance of 80 km from the source calculated using the EPAK-S model of the Finnish Meteorological Institute.

Effective release height, 12.5 m; $v_d = 0.8$ cm s^{-1}

	Wind speed class[a]			
Stratification type	$\bar{u}_1$	$\bar{u}_2$	$\bar{u}_3$	$\bar{u}_4$
Unstable	0.43	0.24	0.18	0.15
Neutral	0.66	0.41	0.33	0.28
Stable	0.76	0.64	0.57	0.51

Effective release height, 75 m; $v_d = 0.8$ cm s^{-1}

	Wind speed class[a]			
Stratification type	$\bar{u}_1$	$\bar{u}_2$	$\bar{u}_3$	$\bar{u}_4$
Unstable	0.34	0.17	0.12	0.10
Neutral	0.47	0.25	0.18	0.04
Stable	0.36	0.14	0.017	0.036

Effective release height, 150 m; $v_d = 0.8$ cm s^{-1}

	Wind speed class[a]			
Stratification type	$\bar{u}_1$	$\bar{u}_2$	$\bar{u}_3$	$\bar{u}_4$
Unstable	0.31	0.14	0.10	0.075
Neutral	0.41	0.19	0.125	0.088
Stable	0.11	0.005	0.0	0.0

Effective release height, 400 m; $v_d = 0.8$ cm s^{-1}

	Wind speed class[a]			
Stratification type	$\bar{u}_1$	$\bar{u}_2$	$\bar{u}_3$	$\bar{u}_4$
Unstable	0.29	0.13	0.08	0.056
Neutral	0.34	0.11	0.055	0.030
Stable	0.0	0.0	0.0	0.0

Effective release height, 150 m; $v_d = 0.2$ cm s^{-1}

	Wind speed class[a]			
Stratification type	$\bar{u}_1$	$\bar{u}_2$	$\bar{u}_3$	$\bar{u}_4$
Unstable	0.11	0.045	0.031	0.023
Neutral	0.17	0.067	0.043	0.030
Stable	0.04	0.0	0.0	0.0

[a] $\bar{u}_1 = 1$ m s^{-1} at 10 m height (z_0); $\bar{u}_2 = 3$ m s^{-1} at 10 m height (z_0); $\bar{u}_3 = 5$ m s^{-1} at 10 m height (z_0); $\bar{u}_4 = 7.5$ m s^{-1} at 10 m height (z_0); $\bar{u}_z = \bar{u}_{z_0}(z/z_0)^p$; $p = 0.12$ (unstable), 0.22 (neutral), or 0.45 (stable).

4.3. FINNISH ESTIMATES OF LOCAL DEPOSITION

During our study of Finnish deposition of sulfur, figures for local deposition were also calculated for different effective release heights, wind speeds, and stability classes. These α' values for total dry deposition are not exactly comparable with the additional deposition values α of the ECE–EMEP model. However, a comparison is nevertheless relevant.

Within an 80 km radius, roughly corresponding to a grid square of 150 × 150 km, the calculated α' values varied from between about 0.0 for high sources, strong wind speed, and stable conditions to 0.76 for low sources, low wind speed, and stable conditions. As may be observed from *Table 4.1*, for a 150 m effective stack height, a wind speed of 5 m s^{-1} at a height of 10 m, and neutral stability conditions, a value of 0.125 was found for α'. For 35 m and 400 m effective stack heights, the corresponding α' figures were 0.25 and 0.055, respectively. These values for dry deposition with a deposition velocity of 0.8 cm s^{-1} agree fairly well with the ECE–EMEP α value of 0.15. However, when the dry deposition velocity changes, the α' value changes considerably. For example, a deposition velocity of 0.20 cm s^{-1} gives a value of 0.043 instead of 0.125 for the 150 m effective stack height case.

REFERENCES

Calder, K.L. (1961), Atmospheric diffusion of particulate matter, considered as a boundary value problem, *J. Meteor.*, **18**(3), 413–416.

Eliassen, A. (1968), The OECD study of long range transport of air pollutants: long range transport modelling, *Atmos. Environ.*, **12**, 479–487.

OECD (1979), *The OECD Programme on Long Range Transport of Air Pollutants. Measurements and Findings*, 2nd edn (OECD, Paris).

Summary of Paper Presented at the International Technical Meeting on *Atmospheric Computations for Assessment of Acidification in Europe: Work in Progress*. Cosponsored by IIASA and IMGW. Warsaw, 4–5 September 1985.

5. A CLIMATIC "STANDARD" SOURCE–RECEPTOR MATRIX

Joop den Tonkelaar
Royal Netherlands Meteorological Institute, Netherlands

5.1. INTRODUCTION

One of the submodels of the IIASA RAINS model is the EMEP Long-Range Sulfur Transport Submodel. The frame of this submodel is a Source–Receptor Matrix (SRM), which describes on an annual basis the atmospheric transport of SO_2 emissions from source areas to dry and wet deposition in the receptor areas.

Originally this *routine* SRM, was based only on the observed meteorology of the *two-year period*, October 1978–September 1980 [1]. However, the *frequency distribution* of the observed general atmospheric circulation patterns during this period deviated from the *long term climatic average* (den Tonkelaar, 1985).

5.2. BASIS OF A CLIMATIC NORMAL MATRIX

Since monthly SRMs are available from the period 1 January 1978–31 October 1982 (58 months) the question arises whether it is possible to construct *standard annual, seasonal, and monthly* SRMs, based on the data of this five-year period, that are in "better" accordance with the long-term climatic frequency distributions of atmospheric circulation patterns than those based on the four-year routine period.

A *climatic normal* frequency distribution has to be based on a 30-year period, with period 1950–1980 recommended by the World Meteorological Organization. Since the frequency distribution of circulation patterns from the 1881–1955 period is also available, both series have been intercompared, in order to determine whether a significant climatic change has occurred or not. Although small deviations between both series exist, mainly due to differences in the determination of the circulation classification during the two periods, these deviations are also part of small climatic fluctuations.

Furthermore, the assumption has been made that the *Standard SRM*, which will be used for the different scenarios until the year 2030, has to

resemble meteorological conditions of the past 30 years. In other words, we assume that no climatic change will occur before 2030.

For the description of the general atmospheric circulation pattern over the area of the East Atlantic and the European continent the classification system of Hess and Brezowsky (1977) has been chosen. This classification is based on a division of climatic patterns into three main types, subdivided into 29 so-called Grosswetterlagen (GWLs). Climatological evidence shows that there are only very weak correlations between the frequency distributions of GWLs from one month to another. This means that the SRMs from month to month may be considered to be meteorologically independent of each other.

To construct *Standard SRMs*, all the 58 available monthly SRMs, or any selection from this number, may be used.

5.3. CONCLUSION

For the construction of a *Standard SRM* it is necessary to select monthly SRMs that improve the frequency distribution of circulation patterns, i.e., a frequency distribution that better corresponds with the climatic normal distribution during the 1950–1980 period. Such a selection has been achieved by subjective "trial and error" by the author. Months that are included and excluded in the proposed "climatic normal" SRM of the "winter-half-year" are presented in *Table 5.1*.

TABLE 5.1. Winter-half-year climatic normal SRM (21 months).

Months	*Included*					*Excluded*				
January		1979	1980	1981	1982	1978				
February	1978		1980	1981	1982		1979			
March		1979		1981	1982	1978		1980		
October		1979	1980	1981	1982	1978				
November	1978	1979	1980							1981
December	1978	1979	1980							1981

An objective approach has also been outlined in den Tonkelaar (1985). Rather than adding months together, as in the above approach, the "objective approach" uses *weighted averages* of months to achieve an SRM that has a "climatic normal" GWL frequency distribution. The procedure for determining weighting factors is described in den Tonkelaar (1985).

NOTE

[1] The RAINS model currently (1985) uses an annual average matrix based on a four-year period (October 1978–September 1982).

REFERENCES

den Tonkelaar, J.F. (1985), *Deposition of Sulfur in Europe: Methods to Construct Unbiased Source-Receptor Matrices from Data of a Limited Period (1976-1982). A Meteorological Contribution to the IIASA RAINS Model*, TR-66, Technical Report [Royal Netherlands Meteorological Institute (KNMI), De Bilt, Netherlands].

Hess, H. and Brezowsky, H. (1977), Katalog der Grosswetterlagen Europas, *Berichte des Deutschen Wetterdienstes*, Nr. 113 (German Weather Service, Offenbach) (in German).

Summary of Paper Presented at the International Technical Meeting on *Atmospheric Computations for Assessment of Acidification in Europe: Work in Progress*. Cosponsored by IIASA and IMGW. Warsaw, 4–5 September 1985.

6. EFFECT OF INTERANNUAL METEOROLOGIC VARIABILITY ON COMPUTED SULFUR DEPOSITION IN EUROPE

Joseph Alcamo and Maximillian Posch
International Institute for Applied Systems Analysis, Austria

6.1. INTRODUCTION

Uncertainty in models used to compute sulfur deposition can originate from a variety of sources (see, for example, Alcamo, 1986). Even if uncertainty due to imperfections of the model are minimal, sulfur deposition computations will still be uncertain due to our inability to anticipate precisely future meteorologic model inputs. This type of uncertainty will arise in the EMEP model of long range sulfur transport and deposition in Europe [1] from the variation of wind and precipitation patterns from year to year. We term this uncertainty "interannual meteorologic variability".

One simple way to investigate this uncertainty is to examine the results of model runs that use meteorological inputs from different years. Streets *et al.* (1985), for example, examined results from the *ASTRAP* sulfur transport model of Eastern North America. In this summary we report on a statistical comparison of results from annual source–receptor matrices of sulfur deposition generated by the EMEP model. The matrix years were:

(1) October 1978–September 1979.
(2) October 1979–September 1980.
(3) October 1980–September 1981.
(4) October 1981–September 1982.

6.2. PROCEDURE

The following steps were followed to conduct the analysis:

(1) Since the effect of interannual meteorological variability will depend on the geographic pattern of sulfur emissions, we selected three scenarios computed by the IIASA RAINS model. These scenarios were selected

because of their large spatial variability and are discussed in Alcamo and Bartnicki (1985).

(2) Each of the four unit-source–receptor matrices is multiplied by each of the three sulfur emission scenarios. This yields four sulfur deposition matrices for each sulfur emission scenario.

(3) The four deposition matrices produced by each sulfur emission scenario are compared on a grid element by grid element basis with the four-year *mean* deposition matrix. The following statistics were used for this comparison:

$$\text{root mean square error } (rmse) = \frac{1}{N}\sqrt{\sum (a_{mn} - b_{mn})^2}$$

$$\text{absolute deviation } (ad) = |a_{mn} - b_{mn}|$$

$$\text{mean absolute deviation } (mad) = \frac{1}{N}\sum |a_{mn} - b_{mn}|$$

$$\text{relative deviation } (rd) = \left|\frac{a_{mn} - b_{mn}}{a_{mn}}\right|$$

$$\text{mean relative deviation } (mrd) = \frac{1}{N}\sum \left|\frac{a_{mn} - b_{mn}}{a_{mn}}\right|$$

where a_{mn} is the grid element of the four-year mean deposition matrix (October 1978–September 1982); b_{mn} is the grid element of the comparison matrix (from matrix years listed in second paragraph of this chapter); and N is the number of grid elements.

6.3. RESULTS

The computed *rmse* ranged from 0.080 to 0.208, depending on the matrix year and sulfur emission scenario. In this application, *rmse* is a measure of which deposition matrix has the largest composite deviation from the mean deposition matrix, i.e., which matrix has the "largest" interannual meteorologic variability. Since the computed *rmse* depends on both sulfur emissions and meteorology, we must be able to estimate the sulfur emission pattern in order to select the "most meteorologically variable" year.

The computed *mad* is summarized in *Table 6.1*, which presents *mad* for the grid elements of three countries and all Europe. (The countries shown are the last three, in alphabetical order, of the 27 largest European countries in Europe.) Results for two of the three sulfur emission scenarios are shown. The absolute deviation, of course, strongly depends on the amount of sulfur emitted. The difference in absolute deviation between the two sulfur emission scenarios shown in *Table 6.1* (a factor of 2 to 3) reflects the difference in total sulfur emissions of the two scenarios.

TABLE 6.1. Summary of computed mean absolute deviations and mean relative deviations.[a]

		Mean absolute deviation ($g\ m^{-2}\ yr^{-1}$)				*Mean relative deviation* (%)			
Scenario	*Country*	(1)	(2)	(3)	(4)	(1)	(2)	(3)	(4)
1980	UK	0.277	0.244	0.261	0.233	10.90	9.61	10.27	9.18
	USSR	0.329	0.374	0.322	0.394	13.06	14.85	12.81	15.67
	Yugoslavia	0.734	0.439	0.442	0.518	15.06	9.00	9.06	10.62
	Europe	0.345	0.317	0.324	0.351	12.92	11.89	12.16	13.18
2010,	UK	0.119	0.100	0.110	0.109	10.58	8.93	9.77	9.68
major	USSR		0.122	0.154	0.125	0.191	13.61	17.21	14.00
pollution	Yugoslavia		0.255	0.154	0.155	0.191	15.13	9.15	9.16
controls	Europe		0.132	0.128	0.127	0.155	12.99	12.60	12.48

[a] (1)–(4) refer to the matrices described in Section 6.1.

The *mrd* is also summarized in *Table 6.1*. As expected, the mean relative deviation is relatively independent of the geographic pattern of sulfur emissions. The mean relative deviation for all grid elements in Europe is approximately 13% and is relatively constant from year to year.

6.4. DISCUSSION

The question arises, do these small differences in computed deposition correspond to small differences in meteorologic patterns between the years 1978–1982? Insight into this question is provided by den Tonkelaar (1985), who has analyzed meteorologic differences between these years by examining the frequency of occurrence of *Grosswetterlagen* (GWL), i.e., synoptic-scale circulation patterns. Since these GWLs are related to precipitation and wind patterns, their frequency of occurrence within a year provides a useful indirect basis for comparing the gross climate patterns of different years. *Preliminary* conclusions of den Tonkelaar's analysis are:

(1) The four-year annual average (October 1978–September 1982) was climatologically similar to the long term (1949–1980) annual average.
(2) The climate patterns of the individual matrix years departed significantly from one another and from the long term average.

In short, GWL records suggest that significant interannual meteorologic variability occurred within the period October 1978–September 1982. However, as we have seen, this variability does not create a large difference in computed patterns of total sulfur deposition when these patterns are averaged over all of Europe and an entire year. There are a number of possible reasons for this:

(1) *The EMEP model is not sensitive to interannual meteorologic changes.* For example, the EMEP model version upon which this chapter is based assumes a constant mixing height throughout the year and from year to year [2]. As a result the EMEP model may "smooth out" differences between computed sulfur depositions that would occur from year to year due to changes in average mixing height. On the other hand, the interannual variation of mixing heights is not known, nor is it known whether this would affect interannual sulfur deposition variability.

(2) *The actual meteorology did not vary much in the years 1978 to 1982.* This would imply that the frequency of GWLs is not a reliable indicator of interannual meteorological variability. One way to check this would be to examine the correlation between wind and precipitation data at several stations and the occurrence of GWLs.

(3) *Deposition is compensated by sulfur emission sources and/or wind and precipitation.* Assuming that the EMEP model adequately incorporates the main effects of interannual meteorological variability on sulfur deposition and that this variability was significant within 1978–1982, then the relatively low variability of sulfur deposition may be due to compensation between sulfur emission sources, i.e., if the prevailing winds transport sulfur from source 'A' to receptor 'B' in one year, then in the next year the prevailing winds from a different direction bring the same amount of sulfur to receptor 'B', but from a different source, 'C'. Another type of compensation could result from meteorological factors. For example, if precipitation at receptor 'B' is much lower than usual during a particular year, the reduction in wet deposition may be compensated by longer range transport of sulfur to this receptor location from more distant sulfur sources.

It is also possible that (1) through (3) occur in some combination.

6.5. CONCLUSIONS

(1) The *rmse* of the computed sulfur deposition matrices depend on the prescribed sulfur emission scenario. Therefore, to identify the matrix with "highest" interannual meteorological variability, we must also estimate the geographic pattern of sulfur emissions.

(2) The absolute deviation in any single grid element spatially varied from about 0.06 to 0.25 g m^{-2} yr^{-1} for the lowest sulfur emission scenario and from about 1.0 to 6.0 g m^{-2} yr^{-1} for the highest

(3) The relative deviation of sulfur deposition in any single grid element varied spatially by about 5–20%.

(4) The average grid element in Europe had a relative deviation of about 13%. This European average was fairly consistent from year-to-year for the four years examined.

NOTES

[1] The EMEP model is discussed further by Alcamo (1986), den Tonkelaar (1986), and Eliassen *et al.* (1986).

[2] Newer versions of the EMEP model are expected to include variable mixing heights.

REFERENCES

Alcamo, J. (1986), A framework for assessing atmospheric model uncertainty, Chapter 1, this volume.

Alcamo, J. and Bartnicki, J. (1985), *An Approach to Uncertainty of a Long Range Sulfur Transport Model*, Working Paper WP–85–88 (International Institute for Applied Systems Analysis, Laxenburg, Austria).

den Tonkelaar, J.F. (1985), *Deposition of Sulfur in Europe: Methods to Construct Unbiased Source–Receptor Matrices from Data of a Limited Period (1978–1982). A Meteorological Contribution to the IIASA RAINS Model*, TR–66, Technical Report [Royal Dutch Meteorological Institute (KNMI), Netherlands].

den Tonkelaar, J.F. (1986), A climatic "standard" source–receptor matrix, Chapter 5, this volume.

Eliassen, A., Lehmhans, J., and Saltbones, J. (1986), Calculated and observed airborne transboundary sulfur pollution in Europe: data covering a five-year period, Chapter 8, this volume.

Streets, D.G., Lesht, B.M., Shannon, J.D., and Veselka, T.D. (1985), Climatological variability, *Environ. Sci. Tech.*, **19**(10), 887–893.

Summary of Paper Presented at the International Technical Meeting on *Atmospheric Computations for Assessment of Acidification in Europe: Work in Progress*. Cosponsored by IIASA and IMGW. Warsaw, 4–5 September 1985.

7. A METHOD TO ASSESS THE EFFECTS OF POSSIBLE CLIMATE CHANGE ON SULFUR DEPOSITION PATTERNS IN EUROPE

S. Pitovranov
All-Union Research Institute for System Studies, USSR

7.1. INTRODUCTION

The increase of CO_2 and trace gas concentrations in the atmosphere, as well as that of other factors of anthropogenic origin, may change the global climate, which could have an impact on sulfur deposition patterns in Europe. Only General Circulation Models (GCMs) distinguish in detail between the atmospheric variables. Unfortunately, present-day GCMs have horizontal mesh scales that are about 500 km or larger, operate with only a steady-state response for a given increase in CO_2, and have some other deficiencies in their description of land-surface hydrology, clouds, surface albedo, and sea ice. Owing to these deficiencies, the computation of temperature change by GCMs is more reliable than other climate variables that they output (Dickinson, 1986). Consideration of energy forecasts, estimates of future CO_2 levels, and computation of the influences of CO_2 and trace gases on the atmosphere's thermal regime, have led to an average forecast of a greater than 1°C global temperature increase by the beginning of the twenty-first century. Changes in regional patterns of climate are much more speculative (Dickinson, 1986). An alternative to using GCMs is to assess future regional climatic changes by using data from historical warming and cooling periods as an analogue, i.e., by assuming that future climate changes will resemble past climate changes.

7.2. HISTORICAL DATA

Historical data have been used to construct precipitation scenarios for Europe in a warmer climate by Lough *et al.* (1983). The mean annual and seasonal temperature, precipitation, and pressure patterns for the warmer 20 years over the period 1934–1953 were compared with the cooler period 1901–1920. According to their assessment, most of Europe received greater

precipitation in autumn and winter during the warm period than during the same months of the cool period. Yet during the spring and summer there was a tendency toward both increased and decreased precipitation in different areas of Europe (*Figure 7.1*).

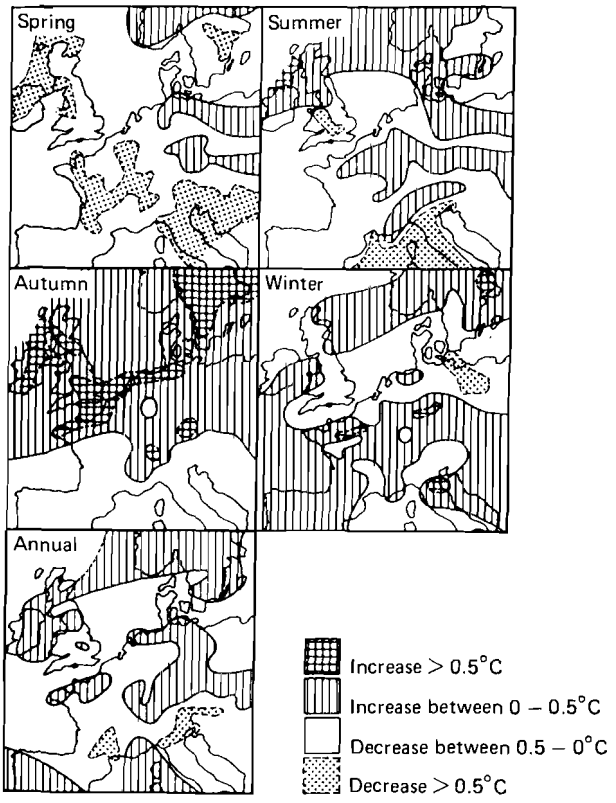

FIGURE 7.1. Changes in precipitation (warm and cold) as multiples of the standard deviation (after Lough *et al.*, 1983).

Not only is precipitation affected by global warming and cooling. Vinnikov and Kovyneva (1983) also show that pressure is very sensitive to the processes of global warming and cooling. For example, *Figure 7.2* shows the atmospheric pressure distribution for the winter season corresponding to a global cooling and global warming of ± 0.5°C.

Historical data can be used to assess the change in sulfur deposition patterns in Europe due to possible future climate change. To do so, we can modify the meteorologic inputs to the EMEP model, i.e., input new wind velocities and precipitation. However, the EMEP model requires much more detailed spatial and time resolution for precipitation and wind patterns than global climate studies normally provide.

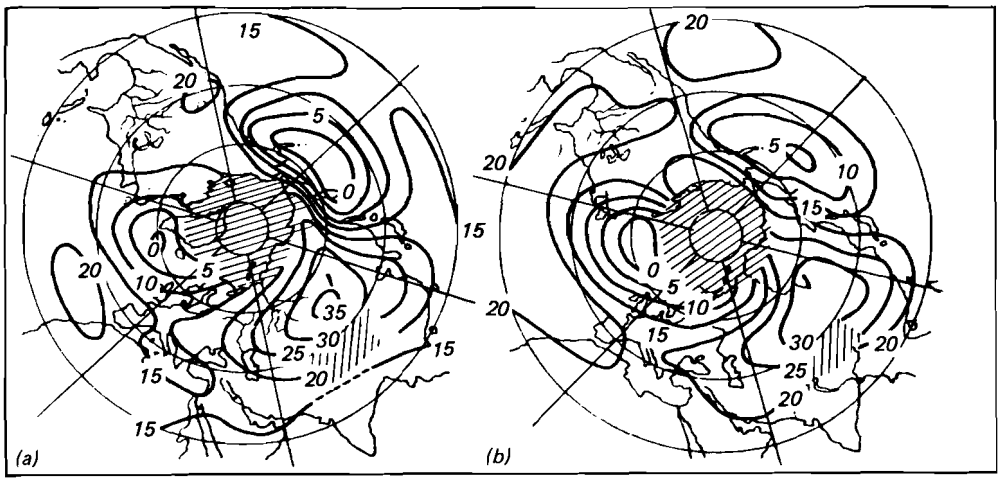

FIGURE 7.2. The atmospheric pressure at sea level for (a) 0.5°C and (b) 0.5°C warming in the extraequatorial belt of the Northern Hemisphere in winter. A standard value of 1000 mb is subtracted. The areas where the estimates are not correct are shaded (after Vinnikov and Kovynava, 1983).

7.3. PROCEDURE

The following procedure can be used to disaggregate information from global climate studies to a scale appropriate for the EMEP model. For this purpose, seasonal values of precipitation and winds must be converted into daily average values. The mean seasonal values can be approximated by trigonometric polynomials under the obvious assumption of annual periodicity. Then, the daily values of these parameters are described by a finite Fourier series given by

$$V_i = C_0 + \sum_{j=1}^{m} C_j \cos\left(\frac{ji}{T} + \Theta_j\right)$$

where V_i is the value of the parameters for day i, C_0 the mean of V_i, $T = 365/2\pi$, C_j the amplitude, and Θ_j the phase angle of the jth harmonic of significance. To determine significant harmonics for each parameter and the maximum likelihood estimates of C_j and Θ_j for each harmonic, we can use the technique described by Woolhiser and Pegram (1979). The experience of simulation modeling shows that for nonlinear models "smoothing" of input data leads to significant errors in output parameters. For example, smoothing of input precipitation data in the EMEP model results in a reduced frequency of the high concentration of sulfate in remote areas (Eliassen and Saltbones, 1983).

To avoid this smoothing problem, we can use a stochastic description of the occurrence of wet and dry days, for which a first-order Markov chain can be used. On days with rain the exponential distribution should describe the amount of rain. The fluctuation of wind may be expressed as

$$u = \bar{u} + \sigma_1 \delta_1(t)$$
$$v = \bar{v} + \sigma_2 \delta_2(t)$$

where $\bar{u}$ and $\bar{v}$ are the smoothed daily meridional and zonal components of wind, σ_1 and σ_2 the standard deviations, and $\delta_1(t)$ and $\delta_2(t)$ functions of time t, representing the realization of a random normal process with zero mathematical expectation and unit variance.

7.4. CONCLUSION

To summarize, first we must obtain scenarios of the Northern Hemisphere mean temperature that correspond to the different possible climate impact scenarios of interest. These temperature data may be obtained from GCM models or other sources. Second, we derive seasonal precipitation and pressure patterns for Europe that correspond to these scenarios of Northern Hemisphere temperature change. This is accomplished by examining the historical relationship between these patterns and the hemispheric temperature, as described above. The next step is to assess the possible seasonal wind patterns that may arise from these seasonal pressure patterns. The final step is to decompose these seasonal estimates of winds and precipitation by the procedure described above into temporal and spatial scales compatible with the EMEP model.

REFERENCES

Dickinson, R.E. (1986), Impact of human activities on climate, in W.C. Clark and R.E. Munn (Eds), *Sustainable Development of the Biosphere* (Cambridge University Press, Cambridge, UK).

Eliassen, A. and Saltbones, J. (1983), Modelling of long-range transport of sulphur over Europe: A two-year model run and some model experiments, *Atmos. Environ.*, **17**, 1457–1473.

Lough, J.M., Wigley, T.M.L., and Paultikov, J.P. (1983), Climate and climate impact scenarios for Europe in a warmer world, *J. Climate Appl. Meteor.*, **22**, 1673–1684.

Vinnikov, K.Ya and Kovyneva, N.P. (1983), On the distribution of climatic changes in global warming, *Meteor. in Gidrolog.*, **N5**, 10–13 (in Russian).

Woolhiser, D.A. and Pegram, G.G.S. (1979), Maximum likelihood estimation of Fourier coefficients to describe seasonal variations of parameters in stochastic daily precipitation models, *J. App. Meteorol.*, **8**(1), 34–42.

PART TWO: STATUS OF LONG-RANGE TRANSPORT MODELS RELEVANT TO DECISION MAKING

Summary of Paper Presented at the International Technical Meeting on *Atmospheric Computations for Assessment of Acidification in Europe: Work in Progress*. Cosponsored by IIASA and IMGW. Warsaw, 4–5 September 1985.

8. CALCULATED AND OBSERVED AIRBORNE TRANSBOUNDARY SULFUR POLLUTION IN EUROPE: DATA COVERING A FIVE-YEAR PERIOD

Anton Eliassen,* Joachim Lehmhaus,** and Jørgen Saltbones* [1]
* *The Norwegian Meteorological Institute, Norway*
** *University of Hamburg, FRG*

8.1. INTRODUCTION

The Co-operative Programme for Monitoring and Evaluation of the Long-Range Transmission of Air Pollutants in Europe (hereafter referred to as EMEP) was started in 1977 and is now one of the key activities under the Convention on Long-Range Transboundary Air Pollution.

The main objective of EMEP is to provide governments with information on the deposition and concentration of air pollutants, as well as on the quantity and significance of pollutant fluxes across national boundaries. The activities of EMEP are divided into a chemical and a meteorological part.

The meteorological part of EMEP is coordinated by WMO, and two Meteorological Synthesizing Centers have been designated. The Meteorological Synthesizing Center, East (EMEP-East) is situated in Moscow, and the Meteorological Synthesizing Center, West (EMEP-West) is situated at the Norwegian Meteorological Institute (NMI). In accordance with its terms of reference, EMEP-West cooperates with the UK Meteorological Office. At EMEP-West, a model for the transboundary transport and deposition of airborne sulfur between 28 European countries has been operated since the beginning of 1978, with simultaneous work on model improvement. In the following, results up to the end of October 1982 are reported, i.e., for a period of 58 months. In addition, attempts were made to detect the sulfur emission reduction which has taken place in most of Western Europe during the period.

8.2. MODEL SPECIFICATION

The receptor-oriented one-layer Lagrangian model operated by EMEP-West has been described in detail elsewhere (Eliassen and Saltbones, 1983) so that only a brief outline is necessary here. The equations for the mass concentrations q and s of SO_2 and particulate sulfate (both measured in sulfur units) are

$$\frac{Dq}{dt} = -\left(\frac{v_d}{h} + k_t + k_w\right)q + \left(1 - \alpha - \beta\right)\frac{Q}{h} \tag{8.1}$$

$$\frac{Ds}{dt} = -\kappa s + k_t q + \beta\frac{Q}{h} \tag{8.2}$$

where D/dt represents the total (Lagrangian) time derivative. The remaining symbols are given in *Table 8.1*. Equations (8.1) and (8.2) are integrated along trajectories followed for 96 hours and arriving at receptors given as grid points in a 150 km grid every six hours. Emissions and six-hourly meteorological fields (winds and precipitation amounts) are given in the same grid.

TABLE 8.1. Parameters in the routine model.

Notation	*Explanation*	*Parameter value*
v_d	Deposition velocity for SO_2	8×10^{-3} m s^{-1}
h	Mixing height	10^3 m
k_t	Transformation rate of SO_2, to SO_4^{2-}	2×10^{-6} s^{-1}
k_w	Wet deposition rate of SO_2, used only in grid elements and six-hour periods when it rains	3×10^{-5} s^{-1}
α	Additional local SO_2 dry deposition on an emission grid square	0.15
β	Part of sulfur emission assumed to be emitted directly as SO_4^{2-}	0.05
κ	Overall decay rate for particulate sulfate	4×10^{-6} s^{-1}

In an alternative model version, the mixing height h is a variable field estimated from radiosonde data, and v_d depends on surface wind speed. In this case, the transformation rate k_t is prescribed to vary seasonally as

$$k_t = 4 \times 10^{-6}\text{s}^{-1} + (2 \times 10^{-6}\text{s}^{-1}) \sin\left(2\pi\frac{t}{T} + \Theta\right) \tag{8.3}$$

where T is one year and Θ is chosen so that k_t has its maximum at the summer solstice. This means that k_t varies between 0.7% per hour in midwinter and 2.2% per hour in midsummer. This model version also has an exchange mechanism between the boundary layer and the free troposphere, whereas the routine model, with a constant mixing height, has an impenetrable lid at the top.

8.3. RESULTS

8.3.1. Quality of Chemical Data

Before comparing calculated and observed data, it is relevant to make some remarks on the quality of the observations. One way of presenting data from the regular interlaboratory comparisons of analytical methods within EMEP is to calculate "scaling factors" for the different laboratories, so that if q_0 is an analytical result from a certain laboratory and q is a "correct value", then $q = \lambda q_0$. Such factors are appropriate if the error is a "scaling error", which often seems to be the case. The λ values are discussed in an EMEP report (Anon, 1984). In addition to analytical errors, there may also be other errors due to, for example, the sampling procedure.

8.3.2. Calculated and Observed Data

Calculations with the simplest model version cover the period from 1 January 1978 to 31 October 1982, a period of 58 months or nearly five years. During the first nine months the precipitation data for the model were incomplete over the south part of the Iberian peninsula. A full set of concentration and deposition maps plus (58-month) average observed SO_2 concentrations plotted against calculated data are given in an EMEP report (Anon, 1984).

There is a reasonable agreement between calculated and observed data, the correlation being slightly lower for precipitation SO_4^{2-} than for the other two quantities. There is a tendency to overpredict high and underpredict low concentrations of SO_2. The EMEP-West allocates a directional transport sector each day at all EMEP stations. The sector allocation is based on the four 96-hour 850 mb trajectories calculated to arrive at the stations each day. Eight transport sectors have been defined (north, northeast, east, ..., northwest).

Figure 8.1 shows calculated and observed mean SO_2 concentrations for each sector for the station DK5. Data are from the 58-month period. This figure shows that, in this case, the directional dependence is well reproduced by the model.

An alternative and somewhat more complex model has been run for the year 1980. The more advanced model has a significantly better correlation at the 1% level and a better prediction of the mean.

8.4. CALCULATED FOUR-YEAR ANNUAL SULFUR BUDGET FOR EUROPE

The resulting calculated four-year annual average country-by-country sulfur budget essentially shows the same situation as the two-year annual budget presented in Eliassen and Saltbones (1983), but is a much better approximation of a longer term climatological average (den Tonkelaar, 1985). Comparing the two budgets, individual matrix elements have changed by 0–30%, the larger relative changes occurring in the smaller elements. Total national depositions have changed by 0–7%.

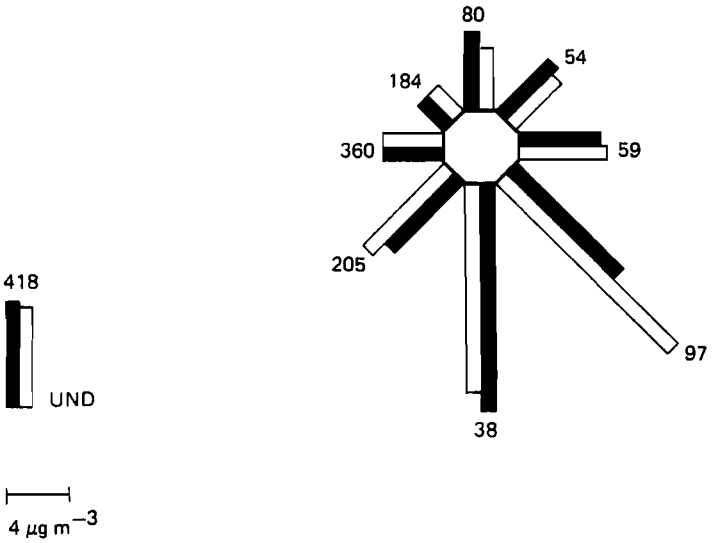

FIGURE 8.1. Observed (black) versus calculated (white) SO_2 mean concentrations in air as a function of transport direction for the station DK5. The length of arms is proportional to average concentration. The number of days in each sector is also shown (totaling 1495), including undecided days (the ninth transport sector) given at the lower left; the observed mean is 5.3, the calculated 5.7 $\mu g\ m^{-3}$.

8.5. ATTEMPTS AT EMISSION REDUCTION DETECTION

EMEP is currently undertaking a new emission inventory for sulfur, in order to update the emission map constructed for 1978 (Dovland and Saltbones, 1979). It is tempting to investigate whether these emission changes can be detected by looking at time series of observed and calculated data.

A difference Δ between an observed quantity q_o and a calculated quantity q_c, the latter being calculated with constant assumed emissions, may indicate whether the emissions Q have increased or decreased in reality. However, Δ gives no information on the magnitude of the change. For this purpose one must rather look at the quantity

$$\delta_1 = 1 + \frac{\Delta}{q_c} \equiv \frac{q_o}{q_c}$$

For a perfect meteorological dispersion model

$$\frac{Q_{\text{real}}}{Q_{\text{assumed}}} \equiv \delta_1$$

In the model calculations, emissions from 1978 were assumed, so that δ_1 should be compared with Q_n / Q_{1978}, n indicating the year. The latter quantity is obviously unity in 1978. For comparison purposes, one should impose the same constraint on δ_1. In other words, one should compare

$$\delta = \frac{q_{o,n} / q_{c,n}}{q_{o,1978} / q_{c,1978}} \quad \text{with} \quad \frac{Q_n}{Q_{1978}}$$

This is done in *Figure 8.2* for the station UK2, since accurate data for annual UK emissions for sulfur are available (Warren Spring Laboratory, communication to EMEP-West). In general, the results for SO_2, particulate SO_4^{2-}, and precipitation SO_4^{2-} seem to confirm the emission reduction in the UK and some nearby countries. The curve for particulate SO_4^{2-} is more irregular than

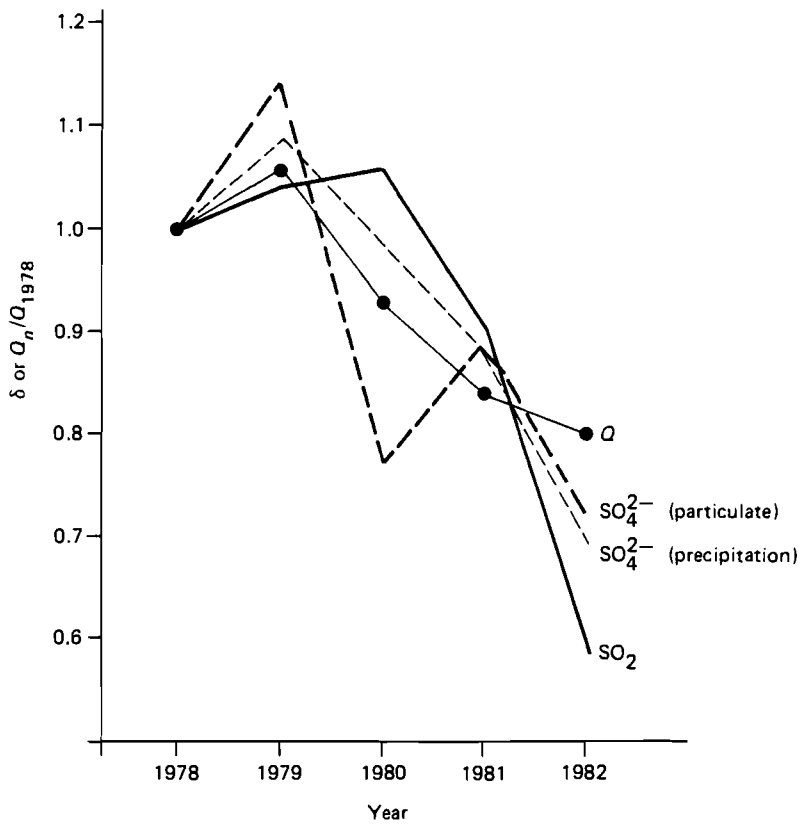

FIGURE 8.2. Normalized ratio between observations and calculations at UK2, plotted against normalized emission development Q for the UK. See text for additional explanation.

the other two, probably reflecting the uncertainty in the general level for these measurements as revealed by the EMEP interlaboratory tests.

ACKNOWLEDGMENT

Mr. Joachim Lehmhaus carried out his part of this work on funding from the Umweltbundesamt of the Federal Republic of Germany, through the University of Hamburg. This generous support is gratefully acknowledged.

NOTE

[1] This summary was prepared by the editors based on the remarks of A. Eliassen and a longer paper with the same title presented by the authors to the Muskoka International Symposium on Acid Precipitation, 15–20 September 1985.

REFERENCES

Anon (1984), *EMEP/MSC-W Report for 1984* (The Norwegian Meteorological Institute, Oslo).

den Tonkelaar, J.F. (1985), *Deposition of Sulfur in Europe: Methods to Construct Unbiased Source-Receptor Matrices from Data of a Limited Period* (1978–1982). *A Meteorological Contribution to the IIASA RAINS Model*, TR-66, Technical Report [Royal Netherlands Meteorological Institute (KNMI), de Bilt, Netherlands]

Dovland, H. and Saltbones, J. (1979), *Emissions of Sulfur Dioxide in Europe in 1978*, Report EMEP/CCC 2/79 [Norwegian Institute for Air Research (NILU), LiUestrom, Norway].

Eliassen, A. and Saltbones, J. (1983), Modeling of long-range transport of sulfur over Europe: a two-year model run and some model experiments, *Atmos. Environ.*, **17**(8), 1457–1473.

Summary of Paper Presented at the International Technical Meeting on *Atmospheric Computations for Assessment of Acidification in Europe: Work in Progress*. Cosponsored by IIASA and IMGW. Warsaw, 4–5 September 1985.

9. THE FIRST PHASE OF AN AUTOMATIC INFORMATION SYSTEM TO CALCULATE TRANSBOUNDARY AIR POLLUTION TRANSPORT

Janna Mikhailova [1]
Institute of Applied Geophysics, USSR

The first phase of a program for calculating transboundary air pollution was devoted to providing routine and summary data of transboundary fluxes of sulfur across the border of the USSR and the countries of the Council for Mutual Economic Assistance (CMEA).

One approach to calculating the sulfur transboundary flux is to use extensive field measurements as a basis. Unfortunately, these measurements do not provide conclusive information about flux direction, nor do they indicate sulfur sources. Moreover, field measurements using the necessary aircraft sampling have been estimated to cost 5–7 million rubles per year. As an alternative to extensive field measurements, the EMEP Meteorological Synthesizing Center East (EMEP-East) has constructed a long-range transport (LRT) model, which computes sulfur transboundary fluxes across the USSR frontier and across an idealized frontier of the CMEA. Field measurements are required to verify this model, but far fewer than the number needed for empirical flux calculations. We estimate that a combined model–field measurement program costs 548 000 rubles less than a field measurement program without modeling.

The model is of the single-layer Lagrangian variety containing semiempirical turbulent diffusion equations and calculates sulfur fluxes and concentrations. Inputs include sulfur emission, six-hour wind speeds, and the amount of precipitation occurring every six hours. Model calculations are compared with aircraft measurements and a small number of ground sampling stations located along border control sites. Model calculations were within actual measurements by a factor of 2–3, which is within the accuracy of field measurements.

Output from the EMEP-East model was compared with that from the EMEP-West model by regression analysis. Monthly computed deposition at several grid points for three separate months were used for this comparison. The correlation coefficients, r, of the regression for April, July, and September 1980 computations were 0.974, 0.948, and 0.948, respectively.

A sample flux calculation produced by the model is shown in *Figure 9.1*. For the one-year period, April 1983 to March 1984, it is estimated that 1.92 × 10^6 t sulfur were transported to CMEA countries across an idealized frontier and 1.42 × 10^6 t in the opposite direction.

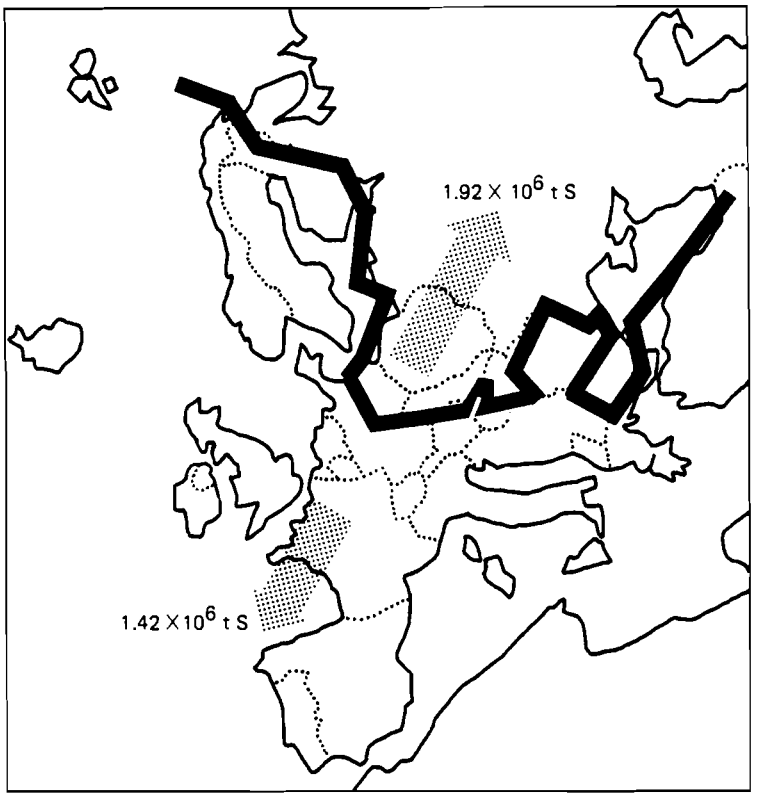

FIGURE 9.1. Net annual flux of sulfur across an idealized border.

In conclusion, the first phase of this program has demonstrated that the flux of sulfur compounds across USSR and other European borders can be estimated with minimum cost and equipment.

NOTE

[1] This summary was written by the editors, based on the presentation of J. Mikhailova.

Summary of Paper Presented at the International Technical Meeting on *Atmospheric Computations for Assessment of Acidification in Europe: Work in Progress*: Cosponsored by IIASA and IMGW. Warsaw, 4–5 September 1985.

10. NONLINEARITY OF THE NO_x SOURCE–RECEPTOR RELATIONSHIP

R. Berkowicz and Z. Zlatev
National Agency of Environmental Protection, Air Pollution Laboratory, Denmark

10.1. INTRODUCTION

An Eulerian Long-Range Transport model has been developed at the Danish Air Pollution Laboratory. The model is designed to provide information on concentrations and depositions of sulfur and nitrogen compounds in Europe on a monthly basis. The transport and transformation processes are described by a one-year, two-dimensional mass-conservation model with linear chemistry involving only sulfur and nitrogen compounds. Sulphur and nitrogen pollutants are, however, treated separately.

The model equations are solved numerically using a pseudospectral method for space discretization. Owing to the very efficient numerical algorithms and a well-structured code, the model can be run through years using only 0.5–1 hour of CPU time per year on, e.g., an IBM 3081 computer (Zlatev *et al.*, 1984).

The model was evaluated against measurements obtained at monitoring stations in Europe and operating within the EMEP network. The results are reported by Zlatev *et al.* (1985a,b). In *Figure 10.1* we show the comparison between measured and computed values for nitrogen using EMEP data from 1979.

10.2. PARAMETERIZATION

The parameters used in the model are estimated by comparing computations with the available measurements. A long simulation process (several hundred model runs) was performed to select the proper formulation of the used parameters.

The parameterization of the physical and chemical processes is similar to that used in the routine EMEP model. However, a seasonal dependence of

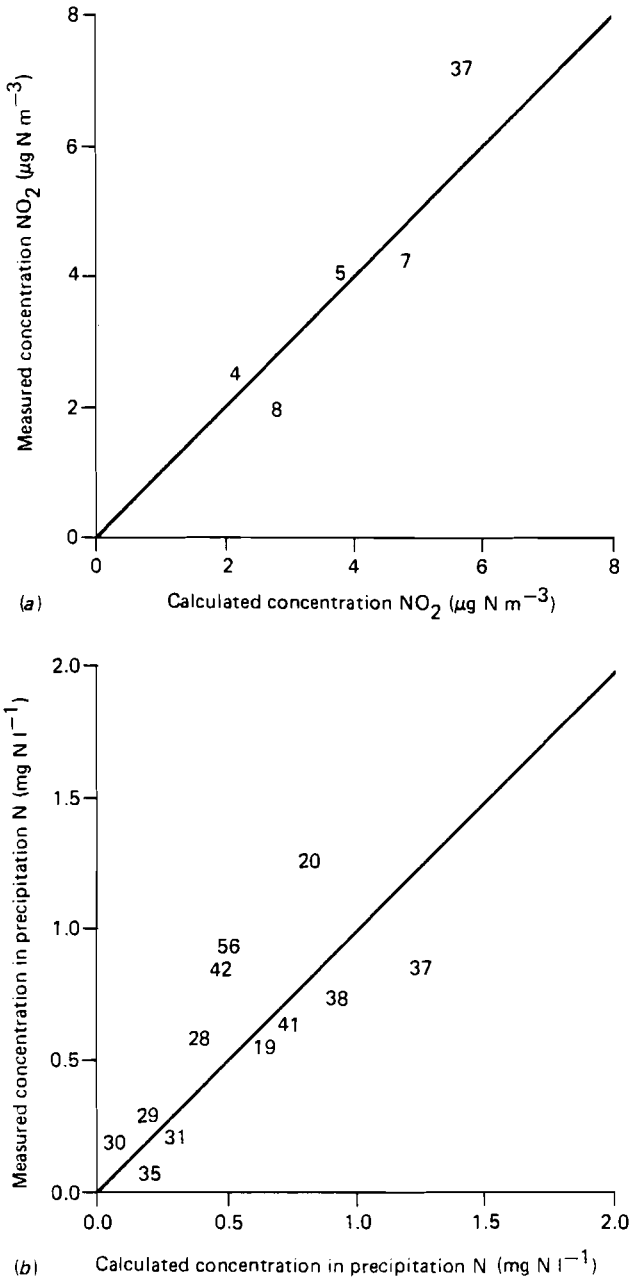

FIGURE 10.1. Comparison of measured and computed concentrations of: (*a*) NO_2 (12-month average, 1979), computed mean 3.79, observed mean 3.93, correlation factor 0.92; (*b*) nitrogen in precipitation (12-month average, 1979), computed mean 0.49, observed mean 0.57, correlation factor 0.76.

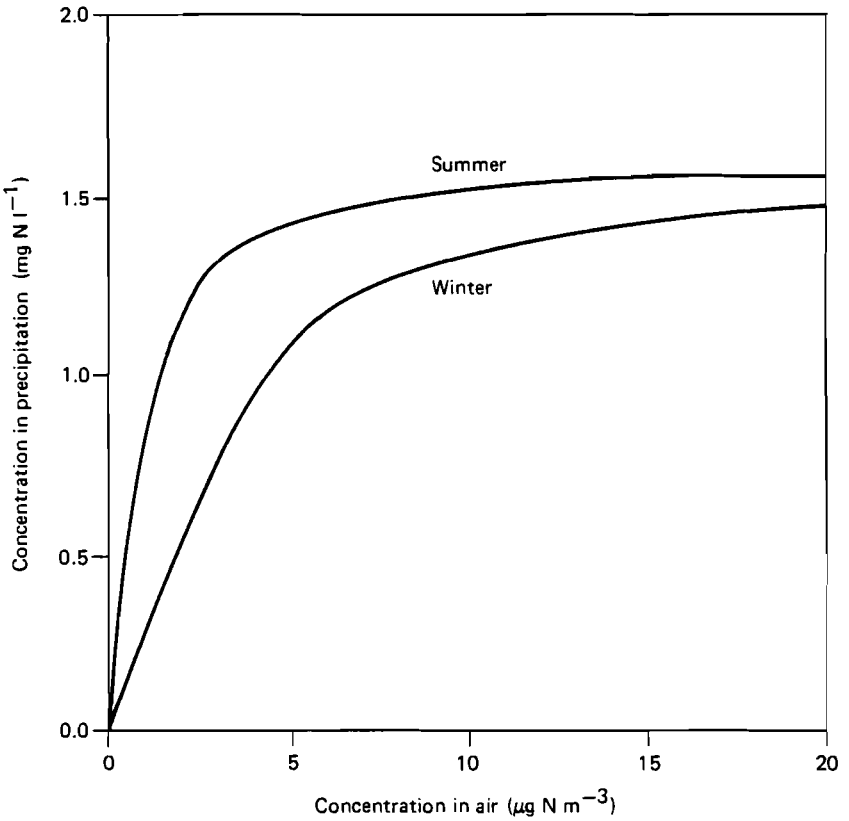

FIGURE 10.2. Concentration in precipitation as a function of total nitrogen concentration in the air. Relationships for the winter and summer periods are shown.

the model parameters is introduced in order to achieve good performance on a monthly basis.

The main innovation introduced in the model is the computational procedure for wet deposition. The amount of pollutants removed from the atmosphere is directly related to the precipitation intensity, but the removal process is nonlinear with respect to air concentrations. The effect of this nonlinearity on the source–receptor relationship for nitrogen is illustrated here by examining the model results.

10.3. NONLINEARITY OF WET DEPOSITION

The NO_3^- concentration in precipitation is modeled by

$$q = ghc \tag{10.1}$$

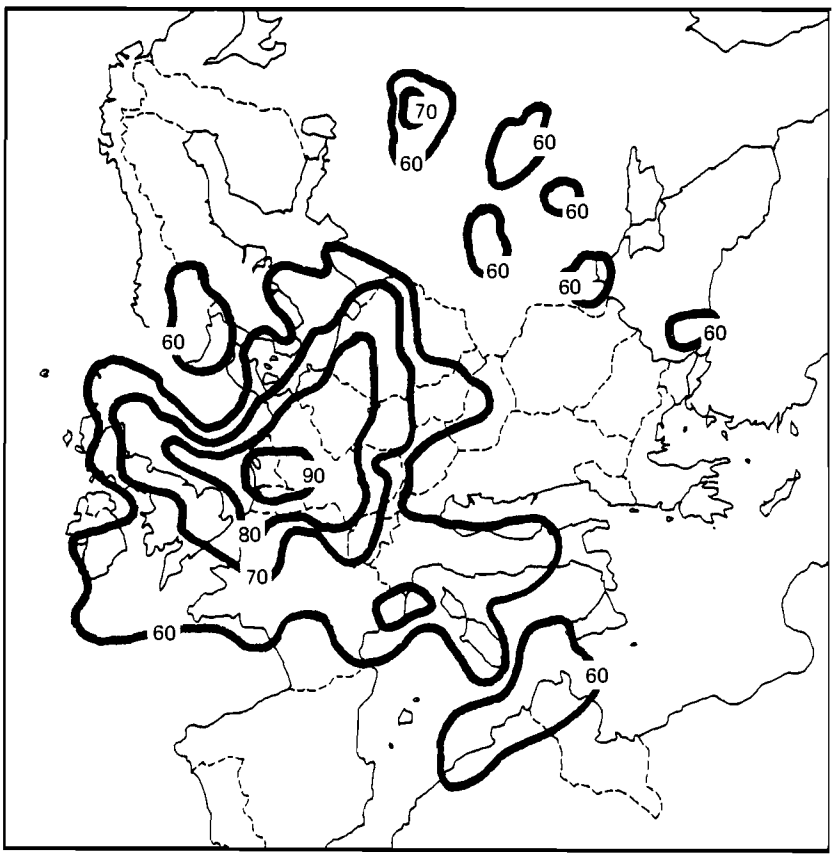

FIGURE 10.3. Ratio (in percent) of January wet nitrogen deposition in 1979 and January wet deposition assuming the emissions are doubled.

where q is the concentration of NO_3^- in precipitation (mg N l^{-1}) and c the total concentration in air of both NO_2 and NO_3^- (μg N m^{-3}). The coefficient g varies through the year, with a minimum in January and December ($g = 0.25$) and a maximum in June and July ($g = 0.75$). The function h depends on c in such a way that it is equal to one for $gc \leq 0.8$ μg m^{-3} and decreases slowly to zero for $gc > 0.8$ μg m^{-3}. In *Figure 10.2* the relationship (10.1) is plotted for the summer and winter periods.

The results shown in *Figure 10.1* were obtained using this nonlinear parameterization of wet deposition. The very good correlation between measurements and model predictions points toward the conclusion that this parameterization is proper. However, at present it is difficult to find an experimental verification of the nonlinearity effect in wet deposition of nitrogen.

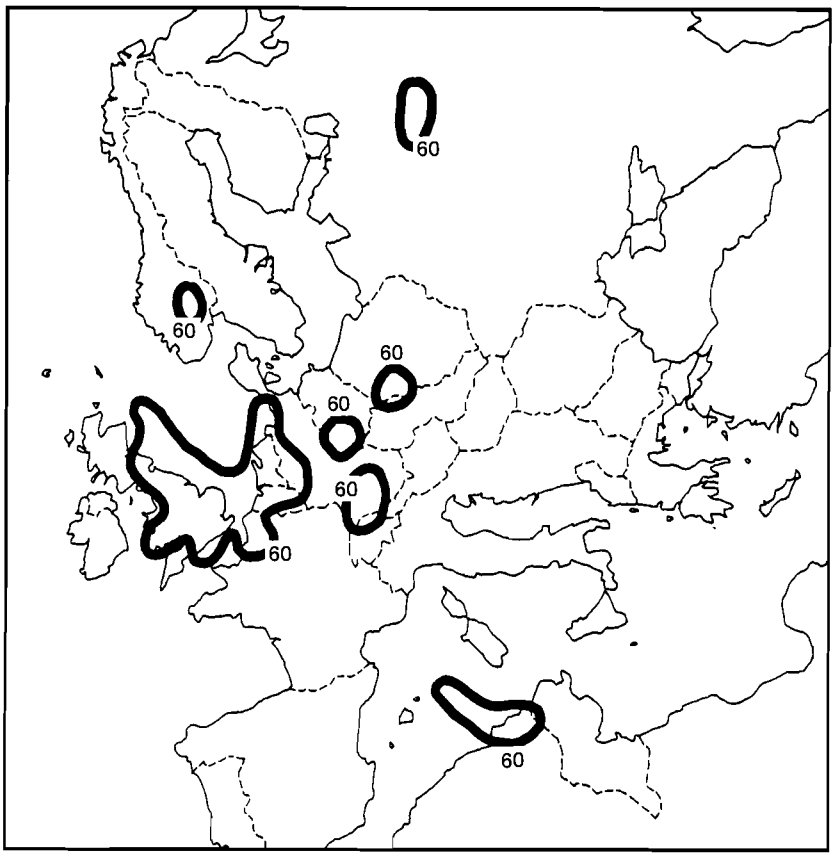

FIGURE 10.4. The same as in *Figure 10.3*, but for total deposition (wet plus dry).

Verification of the model results on measurements from several years with significantly varying emissions could provide information as to the correctness of this nonlinear procedure for wet deposition. Until this verification has been performed, all the results shown here should be considered only as an indication of a problem.

10.4. RELATIONSHIP BETWEEN EMISSION AND DEPOSITION

In order to illustrate the effect of nonlinearity on the emission–deposition relationship we have performed computations of nitrogen deposition with different emission scenarios. The nitrogen emission inventory for 1979 (Semb and Amble, 1981) is used as a reference. Only one month, January 1979, is investigated here.

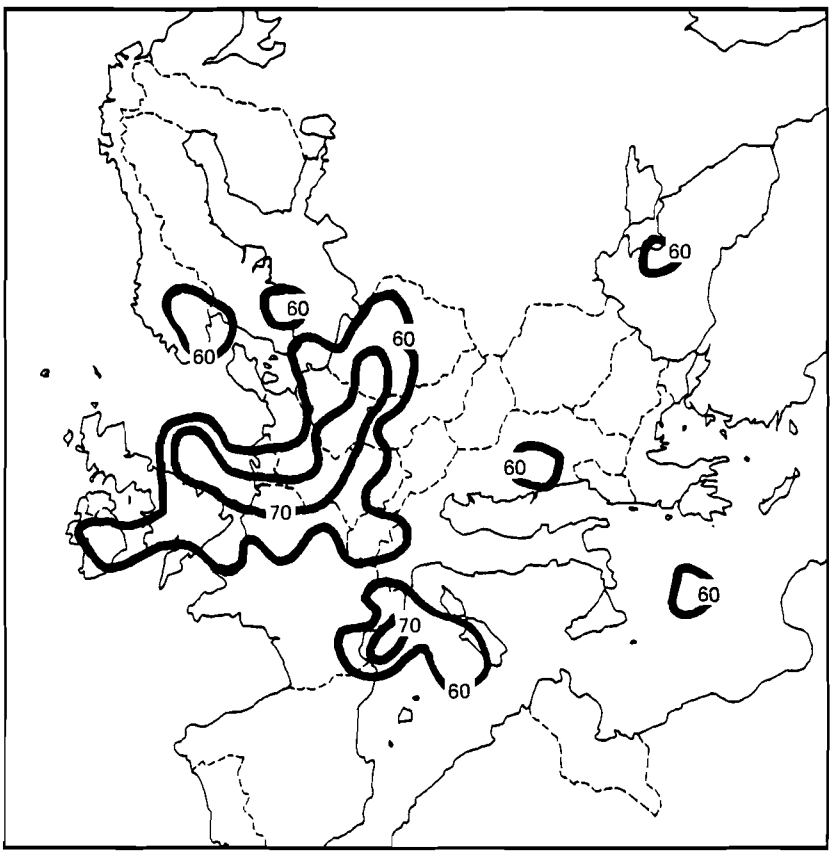

FIGURE 10.5. Ratio (in percent) of January wet nitrogen deposition in 1979 and January wet nitrogen deposition, assuming the emissions are halved.

Figure 10.3 shows the ratio of January wet deposition (in percent) in 1979 with respect to a scenario in which all the emissions are doubled with respect to 1979 emissions. As seen from this figure, in a large part of Central and West Europe the wet deposition in 1979 is more than 60% of the wet deposition corresponding to a doubling of emissions. Close to the largest source area, the ratio is even larger than 90%. In *Figure 10.4*, corresponding results are shown for the total deposition (dry plus wet). Here, the nonlinearity effect is not so strong because the contribution from dry deposition is almost linear. The ratio 60% is exceeded only close to the largest sources. In *Figure 10.5* the changes in wet deposition are investigated for the case of halving the emission with respect to the 1979 level. Comparing *Figure 10.5* with *Figure 10.3* one can conclude that halving the emissions leads to a more linear effect on wet deposition than does doubling the emissions. The changes in total deposition are shown in *Figure 10.6*.

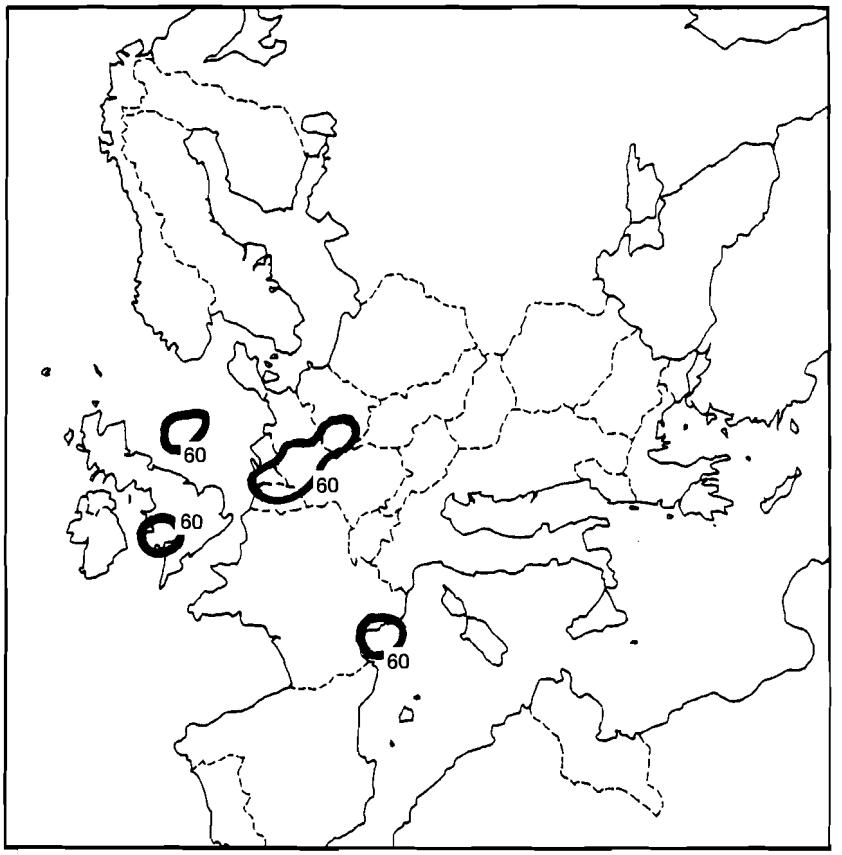

FIGURE 10.6. The same as in *Figure 10.5*, but for total deposition (wet plus dry).

The nonlinearity in wet deposition imposed in the model thus results in a nonlinear emission–deposition relationship. The nonlinearity increases with increasing emissions.

REFERENCES

Semb, A. and Amble, E. (1981), *Emission of Nitrogen Oxides from Fossil Fuel Combustion in Europe*, Report No. 13/8 [Norwegian Institue for Air Research (NILU), Lillestrøm, Norway].

Zlatev, Z., Berkowicz, R., and Prahm, L.P. (1984), Package ADM for studying long-range transport of pollutants in the atmosphere, in B. Engguist and T. Smedsaas (Eds), *PDE Software: Modules, Interfaces and Systems*, pp 153–169 (North-Holland, Amsterdam).

Zlatev, Z., Berkowicz, R., and Prahm, L.P. (1985a), *Studying the Sulfur Pollution in Europe*, MST LUFT-A98 (Air Pollution Laboratory, Danish Agency of Environmental Protection, Risø National Laboratory, Roskilde, Denmark).

Zlatev, Z., Berkowicz, R., and Prahm, L.P. (1985b), *Studying the Nitrogen Pollution over Europe: I. Description of the Model and Some Simple Tests*, MST LUFT (to be published).

Summary of Paper Presented at the International Technical Meeting on *Atmospheric Computations for Assessment of Acidification in Europe: Work in Progress*. Cosponsored by IIASA and IMGW. Warsaw, 4–5 September 1985.

11. A METHOD TO INCLUDE OXIDANTS IN A NO_x LONG-RANGE TRANSPORT MODEL

R.M. van Aalst
TNO, Division of Technology for Society, Netherlands

11.1. INTRODUCTION

IIASA is interested in using a nitrogen oxides (NO_x) long-range transport model to calculate the annual average concentration and deposition of NO_x in Europe. Although NO_x is emitted mainly in the form of NO, the concentration of NO_2 resulting from these emissions is interesting for acid rain modelers because:

(1) Wet and dry deposition of NO_2 are much more important than those of NO.
(2) Chemical conversion of NO_x into HNO_3 and NO_3 occurs almost exclusively via NO_2.
(3) Adverse effects of NO_2 on vegetation occur at much lower concentrations than do those of NO.

In view of the last point, daylight concentrations of NO_2 are particularly relevant; most of the NO_2 enters the plant via the stomata, which are closed at night.

11.2. RELATIONS BETWEEN THE CONCENTRATIONS OF NO_2 AND NO_x

In well-mixed ambient air, the concentrations of NO, NO_2, and O_3 obey the well-known photostationary state relationship:

$$\frac{[NO]\cdot[O_3]}{[NO_2]} = K \qquad (11.1)$$

Here, brackets indicate concentration and K is given by:

$$K = k_1 / k_2$$

where k_1 and k_2 are the rate constants of the reactions:

$$NO_2 \xrightarrow{h\nu} NO + O \xrightarrow{O_2} NO + O_3 \tag{11.2}$$

$$NO + O_3 \longrightarrow NO_2 + O_2 \tag{11.3}$$

k_1 is proportional to the UV-light intensity; at 100 W m^{-2} $k_1 \cong 0.4$ min^{-1}. k_2 is given by $k_2 = 27$ ppm^{-1} min^{-1} at 25°C (Atkinson and Lloyd, 1984). Relationship (11.1) may be rewritten as:

$$\frac{[NO_2]}{[NO_x]} = \left[1 + \frac{K}{[O_3]}\right]^{-1} \tag{11.4}$$

where, by definition:

$$[NO_x] \equiv [NO] + [NO_2] \tag{11.5}$$

In these relationships, the concentrations are expressed in ppbv.

Owing to reactions (11.1) and (11.4), $[O_3]$ is lowered in the neighborhood of sources of NO; however, the concentration of oxidant, defined as:

$$[Ox] \equiv [NO_2] + [O_3] \tag{11.6}$$

remains constant. Eliminating [NO] and $[O_3]$ from equations (11.1), (11.4), and (11.6) and solving for $[NO_2]$, we find:

$$[NO_2] = 0.5([NO_x] + [Ox] + K) - \left\{([NO_x] + [Ox] + K)^2 - 4[NO_x][Ox]\right\}^{0.5} \tag{11.7}$$

Van Egmond *et al.* (1982) tested the validity of these relationships for hourly averaged concentrations in ambient air, measured at stations not directly influenced by emissions of NO. For two series of 744 measurements in the months January and July 1980 they found:

Jan. 1980: $[NO_2]_{meas.} = 0.13$ ppb + 0.99 $[NO_2]_{calc.}$ Standard error = 1.0 ppb
July 1980: $[NO_2]_{meas.} = 1.28$ ppb + 0.95 $[NO_2]_{calc.}$ Standard error = 1.4 ppb

In the calculations K was taken as $0.08\,Q$, where Q is the hourly integrated global radiation in J m^{-2}. However, NO_2 concentrations were generally lower than predicted by equation (11.7) in urban areas and in the vicinity of sources of NO. This may be explained by incomplete mixing of NO-rich parcels with the surrounding air.

The results of the Dutch National Air Quality Monitoring Network also show a complementary character of O_3 and NO_2 in yearly averages. The yearly averaged concentration of oxidant does not show much variation over the Netherlands, indicating its long-range character.

Recently, van Egmond and Kesseboom (1985) showed the validity of equation (11.7) for seasonal averages and used this relationship successfully in calculating long-term averages of NO_2 and NO_x in a model of area 400 × 400 km^2.

The ratio $[NO_2]/[NO_x]$ may differ considerably from unity. Taking as an example $[NO_x] = 5$ ppb and $[Ox] = 20$ ppb we find from equation (11.7) that $[NO_2]/[NO_x] = 0.47$ at $K = 20$ ppb (a sunny day in summer) or $[NO_2]/[NO_x] = 0.68$ at $K = 8$ ppb (a clear day in spring or fall).

11.3. MODELING OF OXIDANT

The ozone or oxidant levels to be used in relationships (11.4) or (11.7) may be derived from measured concentrations. But in predictive modeling applications this procedure is not satisfactory. However, oxidant concentrations may also be calculated from emissions. Long-range transport models for ozone and oxidant are available (USEPA, 1983) and are currently applied to Europe (Meinl and Builtjes, 1984). These models are rather sophisticated and require considerable effort to prepare inputs and calculate results. We advocate here the use of a simple photochemical model for the calculation of oxidant concentrations. Photochemical oxidant-generation occurs mainly by oxidation of hydrocarbons by hydroxyl radicals. Highly schematically, this oxidation may be written:

$$RH + OH \xrightarrow{O_2} RO_2 + H_2O \qquad (11.8)$$

$$RO_2 + NO \longrightarrow NO_2 + RO \qquad (11.9)$$

$$RO \xrightarrow{O_2} RCHO + HO_2 \qquad (11.10)$$

$$HO_2 + NO \longrightarrow NO_2 + OH \qquad (11.11)$$

where RH is a hydrocarbon, RCHO an aldehyde or ketone, and RO_2 an organic peroxy radical. The oxidant formed by reactions (11.9) and (11.11) may be

converted into ozone by reaction (11.2). This reaction sequence may be written in the form:

$$RH + OH \xrightarrow{NO} 2Ox + RCHO + OH \qquad (11.12)$$

The rate of this reaction may be taken as equal to that of reaction (11.8), since reactions (11.9)–(11.11) are much faster under normal ambient conditions.

Reaction (11.12) has the same form as the main reactions that convert SO_2 and NO_x:

$$SO_2 + OH \rightarrow H_2SO_4,\ SO_4^{2-} \qquad (11.13)$$

$$NO_2 + OH \rightarrow HNO_3,\ NO_3^- \qquad (11.14)$$

Although the concentration of OH in ambient air is not well known, estimates used in models for SO_2 and NO_x (van Aalst and Diederen, 1985) may be used for a long term photochemical model as well.

For low concentrations of NO, radical–radical recombination processes impede the formation of oxidant and the regeneration of OH via reaction steps (11.9) and (11.11). These processes may be accounted for by writing:

$$RH + OH \rightarrow \varepsilon Ox + RCHO + p\,OH \qquad (11.12a)$$

where ε and p are dependent on the concentration of NO and on the reactivity and concentration of the organic compound mix. In modeling applications, an effective value could be chosen for ε. Similar simplified reactions may be formulated for other species, such as aldehydes. Results from modeling studies in which such simplified reactions are used compare well with results obtained by using full chemical schemes (van Aalst, 1982).

We therefore propose to use reaction (11.12a) in a long-range transport model, such as used for NO_x, to calculate long-term averaged oxidant concentrations in Europe. Hydrocarbon emissions have to be known by classes of reactivity, according to carbon bond or other schemes. Losses of oxidant by dry deposition or by chemical conversion of NO_2 have to be taken into account, and background levels of ozone must be known.

Note that the concentration of ozone, which is relevant in assessing the direct impacts on vegetation may be calculated directly from the modeled concentrations of NO_x and Ox by using relationships (11.6) and (11.7).

REFERENCES

Atkinson, R. and Lloyd, A.C. (1984), Evaluation of kinetic and mechanistic data for modeling of photo-chemical smog, *J. Phys. Chem. Ref. Data*, **13**, 315.

Meinl, H. and Builtjes, P.G.H. (1984), *Photochemical Oxidant and Acid Deposition Model Application (PHOXA)*, Program of joint projects, FRG–Netherlands.

USEPA (1983), *Proceedings of the US EPA/OECD International Conference on Long Range Transport Models for Photochemical Oxidants and Their Precursors*, EPA-600/9-84-006 (US Environmental Protection Agency, Research Triangle Park, NC).

van Aalst, R.M. (1982), *Voorstudie voor de Berekening van Lange Termijn Gemiddelde Concentraties van Oxidant (Feasibility Study for the Calculation of Long Term Average Concentration of Oxidant)*, Concept-rapport (TNO-MT, Delft, Netherlands).

van Aalst, R.M. and Diederen, H.S.M.A. (1985), Removal and transformation processes in the atmosphere with respect to SO_2 and NO_x, in S. Zwerver and J. van Ham (Eds), *State of the Art of Interregional Modeling* (Plenum Press, London).

van Egmond, N.D. and Kesseboom, N. (1985), A numerical mesoscale model for long-term average NO_x and NO_2-concentration, *Atmos. Environ.*, **10**, 587.

van Egmond, N.D., Kesseboom, N., and van Aalst, R.M. (1982), *Relations Tussen NO_2-, NO- en O_3-Niveaus in de Buitenlucht; Afleiding van een NO_x-Grenswaarde (Relations Between NO_2-, NO- and O_3-Levels in Ambient Air; Derivation of a Limit Value for NO_x)*, RIV-report 227905050 (Rijksinstituut voor de Volksgezondheid, Bilthoven, Netherlands).

PART THREE: LINKAGE BETWEEN ATMOSPHERIC AND ECOLOGICAL MODELS

Summary of Paper Presented at the International Technical Meeting on *Atmospheric Computations for Assessment of Acidification in Europe: Work in Progress*. Cosponsored by IIASA and IMGW. Warsaw, 4–5 September 1985.

12. THE INTERFACE BETWEEN ATMOSPHERIC AND ECOLOGICAL MODELS – THE FOREST ECOLOGIST'S PERSPECTIVE

Annikki Mäkelä
International Institute for Applied Systems Analysis, Austria

12.1. INTRODUCTION

When modeling air-pollutant impacts on a long-term regional basis, a problem of scale arises in the interface between the atmosphere and forest. The EMEP model [1], for instance, produces atmospheric variables as averages over grids amounting to 150 × 150 km^2, while the foresters, accustomed to thinking in units of hectares rather than square kilometers, find significant environmental variation even over a single forest stand. Similarly, the temporal resolution of the output of a regional atmospheric model is bound to be coarse in comparison with the detailed experimental setups that frequent the ecophysiological literature on air pollutant impacts on trees and forests. Given this state of affairs, it is obvious that aggregation of the biological information is required if a match with any large-scale atmospheric model is desired. In this chapter the appropriate methods of aggregation and the consequent requirements on the atmospheric input to the forest submodel used in the IIASA Acid Rain Project are discussed. This submodel is part of IIASA's Regional Acidification INformation and Simulation (RAINS) system.

The Acid Rain Project applies a class of forest models that describe the growth of a stand on an individual tree basis and use an annual time step (Shugart, 1984; Mäkelä and Hari, 1985). Pollutant impact is incorporated in the annual growth increment of each tree as a multiplying factor. As a first step, the impacts of the ambient SO_2 concentration are considered. The "interface problem" is, therefore, to find an appropriate description of the ambient SO_2 concentration, such that the annual, individual tree-based pollutant–growth relationship is as consistent as possible with theory and observation.

12.2. MODEL INPUTS

The impacts of an ambient SO_2 concentration on growth take place through physiological processes. Photosynthesis becomes partially inhibited (Keller, 1978) and the cuticular wax undergoes erosion, enhancing foliage aging (Cape and Fowler, 1981). The intensities of such impacts change temporally over the growing season, depending on the physiological activities of the trees, and spatially over the crown of the individual tree, depending on the microclimate within the canopy. An ideal way of calculating the degree of impact would therefore be to use a submodel with a higher spatial and temporal resolution. Given the current understanding of impact mechanisms, however, the uncertainty introduced through the necessary guesswork would most probably exceed the uncertainty removed through the increased accuracy of the input. Therefore, this approach hardly seems feasible.

A more feasible choice for input as regards temporal scale is a weighted seasonal average. The weights should be estimated on the basis of biological knowledge. If the shape of the seasonal distribution does not vary considerably, the weighted average becomes directly proportional to the annual mean, allowing one simply to use this as a driving variable. In order to judge whether this is feasible, information is required from atmospheric scientists about the inter-annual and regional changes of the intraannual variation.

There are two levels of spatial variation that the atmospheric input has to account for. First, if the SO_2 concentration above a forest stand is known, one would like to know how trees of different sizes are subject to its impacts. The significant size characteristic in the models considered is tree height relative to the remaining canopy. This factor has an impact on the shading of light also, and therefore is an important indicator of the tree's competitive status.

Second, the resolution of input has to match the scale of natural variation in the above-stand SO_2 concentration. Among the most important factors that cause variation in the environment of forests in Central Europe are altitudinal changes. These are extremely important from the pollutant-impact perspective, because the occurrence of damage seems to correlate with altitude (Materna, 1983). In order to be able to judge to what extent this correlation is due to changes in the natural environment only and also to what extent the pollutant load correlates with altitude, the atmospheric models should be developed so as to account for the possible impacts of altitude on the pollutant fluxes.

12.3. CONCLUSIONS

In summary, the modeling of long-term regional air pollutant impacts on forests (as in the forest modeling approach applied in the RAINS framework) requires the following information about the ambient SO_2 concentrations:

(1) Temporal scale:

   (a) Annual average.
   (b) Seasonal relative distributions.

(2) Spatial scale:

   (a) Within stand: concentration above canopy; relative vertical distribution in the canopy.
   (b) Between stand: dependence of concentration on altitude (e.g., within a grid element in the EMEP model).

NOTE

[1] The EMEP model is described in Eliassen and Saltbones (1983).

REFERENCES

Cape, J.N. and Fowler, D. (1981), Changes in epicuticular wax of *Pinus Sylvestris* exposed to polluted air, *Silva Fennica*, **15**(4), 457–458.

Eliassen, A. and Saltbones, J. (1983), Modeling of long-range transport of sulfur over Europe: a two-year model run and some model experiments, *Atmos. Environ.*, **17**(8), 1457–1473.

Keller, T. (1978), Einnfluss niedriger SO_2 Konzentrationen auf die CO_2 Aufnahme von Fichte und Tanne, *Photosynthetica*, **12**(3), 316–322.

Mäkelä, A. and Hari, P. (1986), A stand growth model based on carbon uptake and allocation in individual trees, *Ecol. Mod.* (in press).

Materna, J. (1983), Beziehungen zwischen der SO_2 Konzentration und der Reaktion der Fichtenbestände, *Aquilo Ser. Bot.*, **19**, 147–156.

Shugart, H.H. (1984), *A Theory of Forest Dynamics. The Ecological Implications of Forest Succession Models* (Springer Verlag, Berlin).

West, D.C., McLaughlin, S.B., and Shugart, H.H. (1980), Simulated forest response to chronic air pollution stress, *J. Environ. Qual.*, **9**(1), 43–49.

Summary of Paper Presented at the International Technical Meeting on *Atmospheric Computations for Assessment of Acidification in Europe: Work in Progress*. Cosponsored by IIASA and IMGW. Warsaw, 4–5 September 1985.

13. LINKAGE OF ATMOSPHERIC INPUTS AND FOREST IMPACTS: AN ATMOSPHERIC SCIENCE PERSPECTIVE

Gode Gravenhorst
Alfred Wegener Institut für Polarforschung, FRG

13.1. INTRODUCTION

Input of acidic substances to the soil and foliage, as well as deposition of atmospheric oxidants onto leaves, are put forward, along with direct fumigation, as primary causes for forest damage in Central Europe. The macroscopic visible symptoms (loss of leaves, color changes of assimilation organs), upon which, to a large extent, estimates of forest damage in Germany are based, are, however, so nonspecific that it is hardly possible to directly blame an individual atmospheric trace substance. The complex net of relationships within the atmosphere– plant–soil system could mask connections between atmospheric trace substances and forest damage. It is, therefore, necessary to evaluate those atmospheric trace substances that could interfere with plant-physiological mechanisms and biochemical interactions between plants and the soil, and to be open to the possibility that other culprits (unknown compounds and interaction mechanisms) have yet to be identified.

13.2. POLLUTANT AND FOREST DAMAGE PATTERNS

The damaged forest zone in Germany seems to have a wide distribution with relative maxima in certain areas. Although this reported symptom pattern may be affected by the variety and age distribution of the trees, forest management, soil properties, etc., it could also point to special atmospheric compounds. The very heterogeneous damage-distribution observed on the small scale (down to individual trees) leaves open the possibility of various coexisting influences. The concentration fields for reactive trace substances have, however, not yet been investigated with high resolution in space and time. The results of extensive measurements in industrialized areas, as well as limited research projects and few rural stations, indicate that average SO_2 and NO_x concentrations in rural areas in Germany are lower by a factor of about

five to ten than those in densely populated regions. This pattern does not seem to be consistent with the broad coverage of forest damage, the highest intensity of which probably does not occur close to industrialized areas. The concentration patterns of compounds that are emitted directly into the atmosphere do not, therefore, correlate well with the pattern of macroscopic visible disease symptoms of the trees. It is, however, quite a difficult problem to quantify forest damage in order to compare it with atmospheric concentration patterns. The relative frequency of trees that are damaged according to specific criteria may be a crude measure.

13.3. SECONDARY POLLUTANTS

Secondary pollutants, which are formed within the atmosphere from primary emissions during their transport away from the source areas, have a concentration pattern that is more likely to explain the damage in remote areas, like the Alps and Black Forest. One of these compounds could be O_3, which can have concentrations above its natural background level due to the reactions of nitrogen oxides and hydrocarbons. The level of O_3 is usually higher in rural areas. Furthermore, in summer, during anticyclonic weather conditions with high incoming radiation, O_3 maxima above natural background levels are often formed at higher altitudes at some distance from the areas of the man-made precursors. This general increase of O_3 with altitude and with distance from direct emission sources resembles in some way the horizontal and vertical distribution of forest damage.

13.4. POLLUTANT FLUX

Airborne concentrations of primary or secondary atmospheric trace substances should, however, not be the main parameter of concern when evaluating forest damage. The flux of matter to the foliage and/or to the ground, and not the airborne concentration, determine the forest impact. One should, therefore, focus attention on the flux of atmospheric constituents from the turbulent boundary layer above the canopy to the plant–soil system. These fluxes are limited by transfer resistances due to turbulent diffusion and to molecular diffusion across a laminar layer, by surface resistance of the epidermis, by stomata and mesophyll resistances, and, for particles, by sedimentation resistance. These resistances act partly in sequence and partly in parallel. Their relative magnitude determines which pathway is taken by a certain trace substance during transfer to the plant–soil system. These different resistances vary in time and space and depend mainly on the physical structure of the earth–atmosphere interface, the biological and chemical state of the vegetation, and the properties of the trace substance itself. If atmospheric resistance is the rate determining factor for the uptake of

gaseous and particulate airborne substances, then wind speed, turbulence intensity, forest structure, and orographic features should be the most important parameters for input estimates. Their influences should, however, be evaluated in the field under realistic conditions, in which irregularities dominate the atmosphere–earth interface.

One example, which demonstrates that airborne concentration may not be positively correlated with atmospheric inputs to forests, was found on Mount Kl Feldberg, about 700 m above the industrialized Rhein–Main area of Frankfurt. *Figure 13.1* illustrates that the sulfur flux to a totally absorbing artificial surface exposed to the outside air (IRMA system) was higher by a factor of about 3–5 on Kl Feldberg than in Frankfurt (Vitze, personal communication), although the airborne sulfur concentration is, by about the same amount, smaller at the mountain station than in the industrial area of Frankfurt.

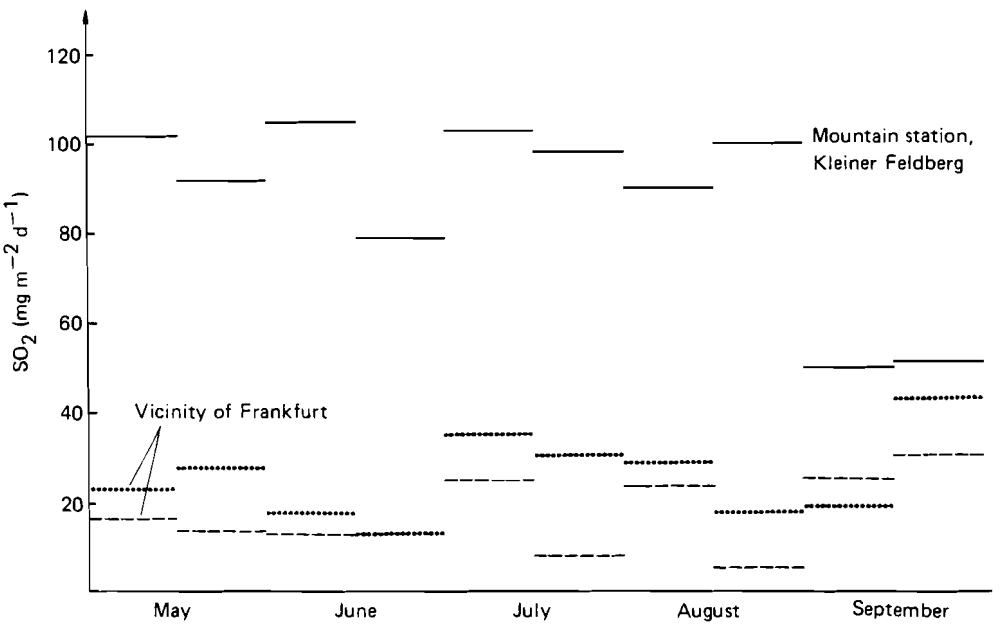

FIGURE 13.1. The amount of airborne sulfur (expressed as SO_2) absorbed by an artificial alkaline wet surface (vertical cylinder, IRMA instrument) at three different sites in the Rhein–Main area. Although the SO_2 concentration is less at the mountain station than at the two sites in the vicinity of Frankfurt, the amount of absorbed sulfur is substantially higher there. These data were measured by Hessische Landesanstalt für Umwelt, Wiesbaden. I thank W. Vitze for his permission to use these unpublished results.

It is, therefore, necessary to evaluate the rate-determining step in uptake of atmospheric constituents by the canopy and the soil. The uptake rates for gaseous and particulate matter in heterogeneous terrain may be quite different and much more structured in time and space than is usually determined in models. This uncertainty may also be important for the

deposition of trace substances incorporated in water droplets. The precipitation deposition of certain substances can be measured satisfactorily if changes in composition during sampling, storage, and analysis are avoided. However, the interception of cloud and fog droplets by the canopy cannot be quantitatively evaluated at the moment. The specific properties of these droplets may be such that they directly damage the assimilation organs and/or that they increase the deposition of acidity to the plant–soil system. How often fog is present at one site can only be a first indication of the potential influence of fog and clouds. The transport of droplets to the foliage increases with wind speed and turbulence, which favors its deposition on vegetation on exposed hills and mountains. This argument does not contradict some features of the broad-scale pattern of forest damage.

Often researchers look for an increase in concentration of specific atmospheric trace substances with time that could account for the reported increase in forest damage within the last decade. This search may be misleading if trace substances (e.g., acidifying substances) gradually reduce the buffer capacity of soil until it is exhausted and unable to withstand further inputs. The concentration of trace substances may even decrease for a long time and nevertheless its deposition cause quite sudden visible damage. How the flux of an atmospheric trace substance develops with time is, therefore, no conclusive indication of a causal relation with forest damage.

13.5. CONCLUSIONS

It seems that an ecosystem – in this case a forest – is such a complex entity and has so many individual appearances that the finely woven net of interactions prohibits simple cause–effect relationships. The result of a single type of research work can probably not explain the observed changes. But it is hoped that the assembly of many different investigations will clarify the overall picture. In this framework atmospheric research can be a valuable part of solving the forest damage problem.

REFERENCE

Vitze, W. personal communication, Hessische Landesanstalt für Umwelt, Wiesbaden.

Summary of Paper Presented at the International Technical Meeting on *Atmospheric Computations for Assessment of Acidification in Europe: Work in Progress*. Cosponsored by IIASA and IMGW. Warsaw, 4–5 September 1985.

14. LINKAGE BETWEEN ATMOSPHERIC INPUTS AND SOIL AND WATER ACIDIFICATION

Juha Kämäri
National Board of Waters, Water Research Institute, Finland

14.1. INTRODUCTION

The IIASA model of acidification in Europe, RAINS (Regional Acidification Information and Simulation), links results from atmospheric long-range transport models with submodels that describe, on the one hand, the production of air pollutant emissions and, on the other, the acidification processes of different parts of the environment. The quantitative link between long-range air pollutant transport and the actual acid load to an environmental system has not been well established. One aspect of this problem is that outputs from atmospheric models often do not coincide with inputs to environmental models.

Environmental acidification models normally require input information on the strong-acid load to the system. Long-range transport models for air pollutants that describe the behavior of transboundary air pollution have given information on mean dry, wet, or total sulfur deposition for large grid squares. For example, the EMEP long-range transport model for sulfur compounds (Eliassen and Saltbones, 1983) assumes a constant deposition velocity over all land surfaces. This assumption seems necessary as the model covers the whole of Europe; it would be an enormous task to describe the spatial variability of dry deposition velocity in detail. In general, the assumption of constant deposition velocity can be supported when modeling the concentration or deposition of sulfur on a large spatial scale. From local experiments it appears, however, that there are significant ecosystem-scale processes that affect the actual amount of acid stress entering the forest floor. The significance of two of these processes, *the filtering effect* and *the deposition of buffering elements*, is discussed in this chapter.

14.2. FILTERING EFFECT

Airborne elements may reach vegetation in aqueous solution or suspension (wet deposition) or as dry particulate or gaseous material (dry deposition). Both

fractions have been defined to involve gravitational deposition, either precipitation or sedimentation, together with an input of material captured from the atmosphere through turbulent transfer and impaction of diffusion (*Figure 14.1*) (Miller and Miller, 1980). This capture, usually termed *the filtering effect* of vegetation (Mayer and Ulrich, 1974), is a function of the aerodynamic and surface characteristics of vegetation (Miller and Miller, 1980). The filtering effect has been clearly demonstrated, for example, in Solling (FRG), where the sulfur load to the spruce ecosystem has exceeded that to neighboring oak and pine stands by more than two (*Table 14.1*) (Matzner, 1983). Thus, although the EMEP long-range transport model produces satisfactory results as far as the variability between the grid squares is concerned, on a local scale it underestimates the deposition on forest land. As forested systems have been the main target for the environmental models of RAINS, it has been considered necessary to include the filtering effect in the models.

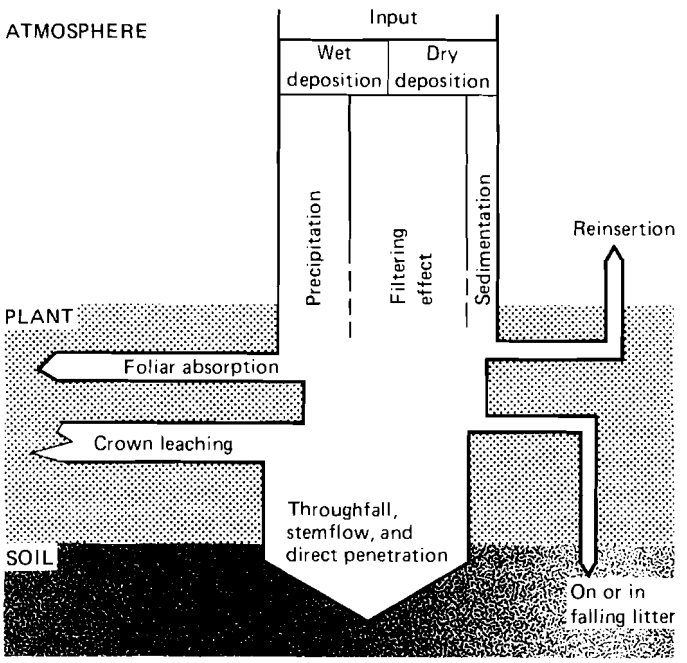

FIGURE 14.1. Pathways for the transfer of atmospheric elements between atmosphere, plant and soil (Miller and Miller, 1980).

The output of the EMEP sulfur-transport submodel of the RAINS model system has been the mean sulfur deposition over a large (150 by 150 km) grid square. Based on validation experiments of the EMEP model, this average total deposition, d_{tot}, has been assumed correct. The deposition on a forest area, i.e., the input to the forest floor, has then been assumed to be φ times larger than the deposition on open land. Defining d_f and d_o as the deposition per

TABLE 14.1. Annual load of sulfur in Solling, FRG, in different ecosystems (kg S ha^{-1} yr^{-1}) (Matzner, 1983).

	Fagus	*Picea*	*Quercus*	*Pinus*	*Heath (open)*
Observation period	1969–1980	1969–1980	1980	1980	1979
Annual S load	52	88	33	35	19

unit area (m^2) on forest and open land, respectively, we can specify the following:

$$d_f = \varphi d_o \tag{14.1}$$

Within one grid square, the total sulfur deposited on forest and on open land has thus been assumed to equal the total input of sulfur over the given grid.

Therefore, since

$$d_{tot} = f d_f + (1 - f) d_o \tag{14.2}$$

where f is the fraction of forest within the grid, we obtain for d_f

$$d_f = d_{tot} \cdot \varphi / [1 + (\varphi - 1) f] \tag{14.3}$$

In *Table 14.2* long-term averages of sulfur bulk deposition and of estimated sulfur input to forest floor (throughfall plus stemflow) are shown for several European ecosystems. This information was used to calculate values for the φ parameter, which gives information on how much the deposition on forest exceeded that on open land. The bulk deposition was here assumed to represent the input to open land. Based on the calculations, the deposition on forest was estimated to be 1.1–3.9 times greater than the deposition assumed for open land. These results, however, are mostly overestimates, since the depositions on open land, on field crops, and on heath are usually greater than the fallout to the bulk collector. This has to do with the greater deposition velocity of gaseous and particulate sulfur material on grass land than on plain bulk collectors. An average factor of $\varphi = 2$ has been used for the whole of Europe, because detailed information on the spatial distribution of φ has not been available (Kauppi *et al.*, 1986). It seems that in remote areas, especially those with high precipitation rates (Scandinavia, Scotland), this value is too large. Yet, in Central Europe, where the total deposition consists to a large extent of dry deposition, the φ value can be, in reality, even larger.

TABLE 14.2. Local observations on sulfur bulk deposition and on total sulfur flux to forest floor, measured as throughfall plus stemflow. Values for the φ parameter were calculated assuming bulk deposition to represent the flux to the open land (see text for further details).

			Observed		
Country/site	*Species*	*Reference*	*Bulk dep.* (kg S ha^{-1} yr^{-1})	*Flux to soil* (kg S ha^{-1} yr^{-1})	φ
FRG/Solling	*Fagus*	Ulrich (1984)	24	50	2.1
France	*Quercus*	Rapp (1973)	16	26	1.6
Poland	*Quercus*	Karkanis (1976)	76	82	1.1
Netherlands	*Quercus/ Betula*	van Breemen *et al.* (1982)	20	61	3.0
Netherlands	*Pinus*	van Breemen *et al.* (1982)	17	60	3.5
Sweden/Jädraas	*Pinus*	Bringmark (1977)	6	8	1.3
Sweden/Jadraas	*Pinus*	Andersson *et al.* (1980)	5	6	1.2
FRG/Solling	*Picea abies*	Ulrich (1984)	22	85	3.9
UK/Kilmichaer	*Picea sitchensis*	Miller and Miller (1980)	30	45	1.5
UK/Leanachan	*Picea sitchensis*	Miller and Miller (1980)	27	49	1.8
UK/Strathre	*Picea sitchensis*	Miller and Miller (1980)	29	49	1.7
UK/Kershope	*Picea sitchensis*	Miller and Miller (1980)	22	40	1.8
UK/Elibank	*Picea sitchensis*	Miller and Miller (1980)	14	29	2.1
UK/Fetteresso	*Picea sitchensis*	Miller and Miller (1980)	20	56	2.0

14.3. DEPOSITION OF BUFFERING ELEMENTS

Acid stress may be defined as the input of effective protons into the top soil. The concept *effective protons* refers to that fraction of total hydrogen-ion input that causes actual soil acidification. Proton input to the system considered may result from deposition of strong acids, from biomass utilization, and from natural biological activity of ecosystems. Any of these sources can dominate the flux of protons entering the soil. When calculating the flux of effective protons, the flux of counteracting ions, the base cations, has to be taken into account. Base cations, mainly Ca^{2+} and Mg^{2+}, contribute to the buffer capacity of the cation exchange system. The atmospheric deposition of base cations is considered to be quantitatively important, so it has been included in the calculation of acid stress.

In principle, all the depositing sulfur atoms are assumed to oxidize and produce sulfuric acid. The total proton flux to the soil can thus be estimated on the basis of sulfur deposition, simply by assuming the proton flux to equal the sulfate ion equivalents in the water entering the soil. The contribution of

base cations to the cation exchange buffering is estimated with the aid of parameter σ, which represents the fraction of total proton flux, d_f, that is not counteracted by base cation deposition, d_{bc} (both in keq ha^{-1} yr^{-1}):

$$\sigma = 1 - \left[\frac{d_{bc}}{d_f}\right] \tag{14.4}$$

One obtains, then, for acid stress, as:

$$as = d_f - d_{bc} \tag{14.5}$$

or

$$as = \sigma d_f \tag{14.6}$$

Base cation deposition strongly depends on the location. In the vicinity of the sea, sea salts increase the deposition of sodium especially. The Gouy theory has, however, pointed out that multivalent ions are concentrated in the cation exchange complex to a much larger extent than monovalent ions. Thus, the Ca^{2+}/Na^{+} ratio is much higher in the proximity of a negatively charged surface than in the medium (see Stumm and Morgan, 1981). The monovalent ions, Na^{+} and K^{+}, preferably remain in soil solution at high ionic strengths and do not significantly take part in the cation exchange reactions. Therefore, the value for σ at different locations in Europe has been estimated from the available literature on the basis of fluxes of divalent cations, Ca^{2+} and Mg^{2+}, only.

The results in *Table 14.3* suggest that σ values do not vary much between different locations in Europe. The value $\sigma = 0.67$, used in earlier applications (Kauppi *et al.*, 1986), seems to be a reasonable approximation for the present effect of base cation deposition on the acid stress. However, in applications to future scenarios the two alternative forms of equations [equations (14.5) and (14.6)] give different results; in equation (14.5) the base cation deposition is assumed independent and in equation (14.6) dependent on the sulfur deposition. Equation (14.5) implies that base cations originate from totally different sources than sulfur, and the base cation deposition will stay at the present level, d_{bc}. If equation (14.6) is assumed valid, then the base cations are mainly emitted in the same processes as sulfur. Either one of these assumptions can presently be included in the IIASA forest soil acidity submodel.

14.4. CONCLUSIONS

The target systems for the acidification studies of IIASA are forests, forest soils, and forested catchments. First attempts to estimate the local proton

TABLE 14.3. Local observations on $Ca^{2+} + Mg^{2+}$ deposition and SO_4^{2-} deposition and, based on these, calculated values for the σ parameter (see text for further details).

Site	*Country*	*Reference*	*Observation period*	$Ca^{2+} + Mg^{2+}$ *deposition* (keq km^{-2} yr^{-1})	SO_4^{2-} *deposition*	σ
Birkenes	Norway	Wright and Johannessen (1980)	1972–1979	45	142	0.68
Fyresdal–Nissedal	Norway	Johannessen and Joranger (1976)	1974–1975	20	79	0.75
Langtjern	Norway	Henriksen (1976)	1973–1975	12	54	0.78
Fillefjell	Norway	Dovland (1976)	1973–1974	7	23	0.70
Solling, Beech	FRG	Matzner (1983)	1969–1980	141	323	0.56
Solling, Spruce	FRG	Matzner (1983)	1969–1980	175	547	0.68
Solling, Oak	FRG	Matzner (1983)	1980	62	207	0.70
Solling, Pine	FRG	Matzner (1983)	1980	69	220	0.69
Solling, Heath	FRG	Matzner (1983)	1979	35	118	0.70
Jädraas	Sweden	Andersson *et al.* (1980)	1984	9	39	0.77

fluxes to the forest floor from regional average depositions have been described in this chapter. Many questions, however, remain to be solved. The following gaps in our understanding of linking atmospheric models to environmental models require a concentrated research effort:

(1) The filtering effect is extremely important in areas where deposition largely occurs as dry deposition. Factors that have a decisive role in this process are the tree species, i.e., the surface characteristics of the capturing vegetation and the amount of dry deposition. Whether there are other factors affecting this filtering or whether reliable results can be obtained on the basis of these two only remains to be examined.

(2) Spatially, the base cation deposition varies markedly. The spatial distribution of base cation deposition, however, tends to follow the spatial sulfur deposition pattern. It is evident that close to the emission sources there occurs high sulfur deposition together with high deposition of dust and other particulate impurities rich in base cations. Therefore, at present, the resulting sulfur/base cation deposition ratio seems to be quite constant. This may, however, be a consequence of intensive human activity of all kinds occurring in the same areas, so the future base cation deposition should probably be independent of sulfur deposition. If this is the case, the deposition of buffering elements will not decrease, even if measures were taken to control sulfur emissions. The unsolved question as to whether the sulfur/base cation deposition ratio is constant

only in space and not in time is important, since this has a significant effect on the rate of recovery for the acidified soils.

REFERENCES

Andersson, F., Fagerström, T., and Nilsson, S.I. (1980), Forest ecosystem responses to acid deposition: Hydrogen ion budget and nitrogen/tree growth model approaches, in T.C. Hutchinson and M. Havas (Eds), *Effects of Acid Precipitation on Terrestrial Ecosystem*, pp. 319–334 (Plenum Press, New York).

Bringmark, L. (1977), A bioelement budget in an old Scots pine forest in central Sweden, *Silva Fenn.*, **11**, 201–209.

Dovland, H. (1976), *Chemistry of Precipitation and River Water, Fillefjell, May 1973–June 1975*, SNSF-project TN 23/76 [Norwegian Institute for Air Research (NILU), Lillestrøm, Norway] (in Norwegian).

Eliassen, A. and Saltbones, J. (1983), Modeling of long-range transport of sulfur over Europe: a two-year model run and some model experiments, *Atmos. Environ.*, **17** (8), 1457–1473.

Henriksen, A. (1976), *Chemical Investigations of Precipitation and River Water in the Langtjern Basin, Southern Norway, 5 May 1973–30 June 1975*, SNSF-project TN 25/76 [Norwegian Institute for Air Research (NILU), Lillestrøm, Norway] (in Norwegian).

Johannessen, M. and Joranger, E. (1976), *Chemical Investigations of Precipitation and River Water in Fyresdal and Nissedal, Southern Norway*, SNSF-project TN 30/76 [Norwegian Institute for Air Research (NILU), Lillestrøm, Norway] (in Norwegian).

Karkanis, M. (1976), The circulation of sulphur in the forest ecosystem *Tilia-Carpinetum* in the northern part of Puszcsa Niepolomicka near Ispira, *Fragm. Florist. Geobot.*, **22**, 351–363.

Kauppi, P., Kämäri, J., Posch, M., Kauppi, L., and Matzner, E. (1986), Acidification of forest soils: model development and application for analyzing impacts of acidic deposition in Europe, *Ecol. Mod.* (in press).

Matzner, E. (1983), Balances of element fluxes within different ecosystems impacted by acid rain, in B. Ulrich and J. Pankrath (Eds), *Effects of Accumulation of Air Pollutants in Forest Ecosystems*, pp. 147–156 (D. Reidel Publ. Co., Dordrecht).

Mayer, R. and Ulrich, B. (1974), Conclusions on filtering action of forest from ecosystem analysis, *Oecol. Plant.*, **9**, 157–168.

Miller, H.G. and Miller, J.D. (1980), Collection and retention of atmospheric pollutants by vegetation, in D. Drablos and A. Tollan (Eds), *Ecological Impact of Acid Precipitation, Proc. of Conf. Sandefjord, March 11–14, 1980*, pp. 33–40, SNSF-project [Norwegian Institute for Air Research (NILU) lillestrøm Norway].

Rapp, M. (1973), Le cycle biogeochimique du soufre dans une foret de *Quercus ilex L.* du sud de la France, *Oecol. Plant.*, **8**, 325–334.

Stumm, W. and Morgan, J. (1981), *Aquatic Chemistry. An Introduction Emphasizing Chemical Equilibria in Natural Waters*, 2nd edn (J. Wiley & Sons, New York).

Ulrich, B. (1984), Effects of air pollution on forest ecosystems and waters – the principles demonstrated at a case study in Central Europe, *Atmos. Environ.*, **18**, 621–628.

van Breemen, N., Burrough, P.A., Velthorst, E.J., van Dobben, H.F., de Wit, T., Ridder, T.B., and Reijnders, H.F.R. (1982), Soil acidification from atmospheric ammonium sulfate in forest canopy throughfall, *Nature*, **299**, 548–550.

Wright, R.F. and Johannessen, M. (1980), Input–output budgets of major ions at gauged catchments in Norway, in D. Drablos and A. Tollan (Eds), *Ecological Impact of Acid Precipitation, Proc. Conf. Sandefjord, March 11–14, 1980*, pp. 250–251, SNSF-project [Norwegian Institute for Air Research (NILU), Lillestrøm, Norway].

Summary of Paper Presented at the International Technical Meeting on *Atmospheric Computations for Assessment of Acidification in Europe: Work in Progress*. Cosponsored by IIASA and IMGW. Warsaw, 4–5 September 1985.

15. THE RELATIONSHIP BETWEEN GROUND LEVEL CONCENTRATIONS AND AVERAGE MIXING LAYER CONCENTRATIONS OF SO_2

R.M. van Aalst* and J.A. van Jaarsveld**

* *TNO, Division of Technology for Society, Netherlands*

** *National Institute of Public Health and Environmental Hygiene, Netherlands*

15.1. INTRODUCTION

In the IIASA RAINS model for acidification in Europe, annual averaged concentrations of SO_2 and deposition of SO_2 and SO_4^{2-} are calculated on the basis of predictions of the routine EMEP-West model of EMEP (Eliassen and Saltbones, 1983). In this model, the emissions of SO_2 are considered to be equally distributed over the mixing layer. However, for the purpose of assessing direct forest impact, IIASA is interested in ground level concentrations. A simple model predicting the average vertical concentration profile in the mixing layer is presented and tested against measurements of SO_2 at the 200 m meteorological tower in Cabauw, Netherlands.

15.2. THEORY

Advection of pollutants and dry deposition may cause vertical concentration gradients in the mixing layer. The advection gradient may be highly variable in the horizontal plane and cannot be accounted for in a simple way by the EMEP SO_2 model. For dry deposition, the concentration profile in the so-called constant flux layer is:

$$c(z) = c(z_r) - F\int_{z_r}^{z} \frac{dz}{K_z} \tag{15.1}$$

where $c(z)$ is the concentration at height z, z_r a reference height, and K_z the vertical turbulent diffusivity. F is the deposition flux:

$$F = -v_d c(z_r) \tag{15.2}$$

where v_d is the deposition velocity. Substitution of equation (15.2) into (15.1) gives:

$$c(z) = c(z_r)\left[1 + v_d \int_{z_r}^{z} \frac{dz}{K_z}\right] \tag{15.3}$$

K_z in the surface layer is given from similarity theory by

$$K_z = \frac{k u_* z}{\varphi_h(z/L)} \tag{15.4}$$

where φ_h is the nondimensional flux profile function for heat, u_* the friction velocity, k von Kármán's constant, and L the Monin–Obhukov length.

15.3. COMPARISON WITH MEASURED PROFILES

Table 15.1 lists semiannual averages of the hourly concentrations of SO_2 and NO_x measured at the Cabauw tower at heights of 4, 100, and 200 m. The data

TABLE 15.1. Average concentrations of SO_2 and NO_x measured at the Cabauw tower from 1 April 1980–1 April 1981.

	$[SO_2]$ ($\mu g\ m^{-3}$)		$[NO_x]$ (ppb)	
Height (m)	*Summer*	*Winter*	*Summer*	*Winter*
4	15	24	21	32
100	23	36	11	23
200	23	39	10	17

show that gradients are largest in the lowest layer. The gradient of NO_x indicates an upward flux as expected for emissions by motor traffic. Earlier analyses of the data for SO_2 at Cabauw (van Dop *et al.*, 1980; Onderdelinden *et al.*, 1984) showed an influence of advection. Recently, Onderdelinden *et al.* (1984) analyzed all SO_2 data gathered during five years of measurements and found abnormally large gradients for southerly and southwesterly winds (see *Figure 15.1*), which could be attributed to emissions from a coal-fired power plant and from an industrial area with oil refineries some tens of kilometres from Cabauw.

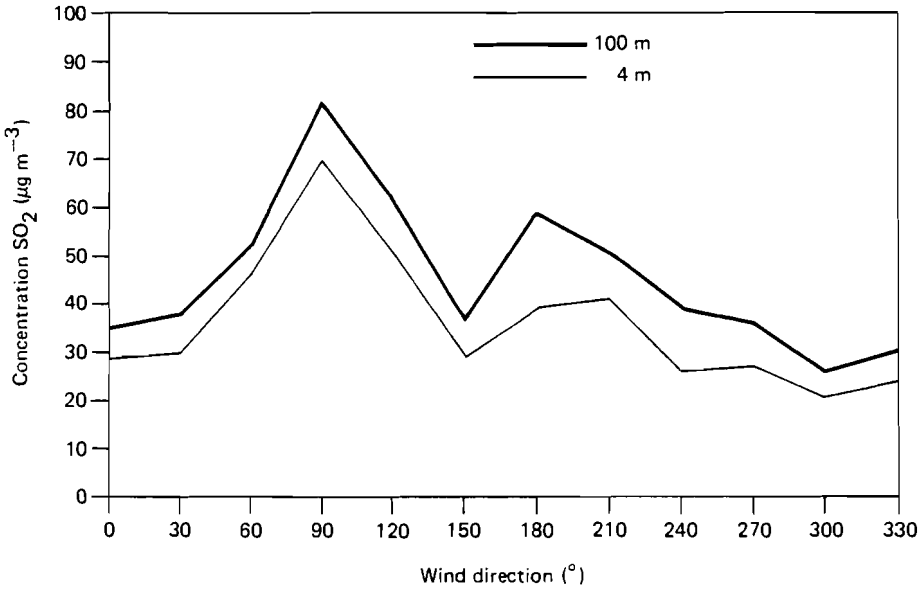

FIGURE 15.1. Average SO_2 concentrations measured at Cabauw at 4 and 100 m in the period 1979–1984 for neutral stability (Class D_m) as a function of wind direction. Concentrations less than 10 $\mu g\ m^{-3}$ have been omitted (from Onderdelinden *et al*, 1984).

Table 15.2 lists average concentrations of SO_2 for all except these wind sectors for the different stability classes. Concentrations below 10 $\mu g\ m^{-3}$

TABLE 15.2. Five-year (1 January 1980–1 January 1985) averages of hourly SO_2 concentrations (in $\mu g\ m^{-3}$) measured at the Cabauw tower. Wind sectors south (180°), west-southwest (240°), and west (270°) and concentrations below 10 $\mu g\ m^{-3}$ are excluded.

Stability class[a]	*Frequency*	*c* (4)	*c* (100)	*c* (200)
A, B, C	0.11	43.8	52.8	52.7
D_l	0.25	35.3	54.3	63.2
D_m	0.27	38.3	47.8	51.3
D_h	0.24	34.4	39.4	38.4
E	0.05	36.3	61.0	74.3
F	0.08	27.9	66.6	75.6
All classes		36.2	50.3	54.6

[a] According to Pasquil. Class D was subdivided into classes of inversion height H. D_l, $H < 250$ m; D_m, 250 m $< H <$ 600 m; D_h, $H > 600$ m.

were omitted in view of the limited resolution (6 $\mu g\ m^{-3}$) of the SO_2 monitors. From similar data, Onderdelinden *et al.* (1984) derived an average deposition

velocity for SO_2 of 0.75 cm s^{-1}, in close agreement with the value of 0.8 cm s^{-1} adopted in the EMEP model. We now compare these data with relations (15.3) and (15.4), using simple assumptions for the dependence of K_z on height, and assuming v_d = 0.8 cm s^{-1}. Values of u_* and L were obtained from observed wind speed and global radiation data at Cabauw and a calculation scheme proposed by Holtslag and van Ulden (1983).

If the Businger relationships:

$$\begin{aligned} \varphi_h &= 0.74(1 - 9z/L)^{-0.5} \quad (L < 0) \\ \varphi_h &= 0.74 + 4.7z/L \qquad\quad (L > 0) \end{aligned} \tag{15.5}$$

are substituted into equation (15.4), the results shown in *Table 15.3* are obtained.

TABLE 15.3. Ratio of average concentrations at heights of 4 m and 100 m as calculated from equations (15.3), (15.4), and (15.5) and as measured, per stability class. The average aerodynamic resistance r_a (= $\int dz/K_z$) between 4 and 100 m is also shown.

	r_a (4, 100)	$c(4)/c(100)$	
Stability class	(m s^{-1})	*Calculated*	*Measured*
A, B, C	7	0.95	0.83
D_l	83	0.60	0.65
D_m	18	0.87	0.80
D_k	9	0.93	0.87
E	62	0.67	0.60
F	604	0.17	0.42
All classes		0.76	0.74

The average profile is described satisfactorily but, for nonneutral conditions, there are fairly large deviations between calculated and observed profiles. These deviations are not unexpected, because relationships (15.4) and (15.5) are valid only for heights of up to about 2 $|L|$.

In the EMEP model no information on stability is available. Therefore, we also considered the simple assumption (see Gillani, 1978):

$$\begin{aligned} K_z &= ku_*z \quad (z < 50 \text{ m}) \\ K_z &= ku_*50 \quad (z \geq 50 \text{ m}) \end{aligned} \tag{15.6}$$

The results are shown in *Table 15.4*.

Although the calculated results are rather different from those listed in *Table 15.3*, the agreement with measured data is still acceptable. The table also gives an estimate of the ratio of the ground level concentration to the

TABLE 15.4. Ratio of average concentration at a height of 4 m to those at 100 m and at 200 m, and to the estimated mixing layer average $\bar{c}_H$. Calculated values were obtained from equation (15.6).

Stability	u_*	$c(4)/c(100)$		$c(4)/c(200)$		$c(4)/\bar{c}_H$
class	(m s^{-1})	*Calc.*	*Meas.*	*Calc.*	*Meas.*	*Calc.*
A, B, C	0.41	0.85	0.83	0.79	0.83	0.68
D_l	0.22	0.76	0.65	0.67	0.56	0.53
D_m	0.47	0.87	0.80	0.81	0.75	0.71
D_h	0.71	0.91	0.87	0.87	0.90	0.79
E	0.32	0.82	0.60	0.74	0.49	0.63
F	0.12	0.63	0.42	0.52	0.37	0.39
All classes		0.83	0.74	0.76	0.70	0.66

mixing layer average calculated from equation (15.3). A constant mixing height of 800 m was assumed. In view of the simplifying assumptions in the derivation of these ratios and the lack of experimental data on average SO_2 concentrations profiles for heights in excess of 200 m, these values must be seen as indications only.

ACKNOWLEDGMENT

All concentration data presented were kindly provided by the National Institute of Public Health and Environmental Hygiene (RIVM).

REFERENCES

Eliassen, A. and Saltbones, J. (1983), Modeling of long-range transport of sulfur over Europe: a two-year model run and some model experiments, *Atmos. Environ.*, **17**(8), 1457–1473.

Gillani, N.V. (1978), Project MISTT: Mesoscale plume modeling of the dispersion, transformation and ground removal of SO_2, *Atmos. Environ.*, **12**, 569.

Holtslag, A.A.M. and van Ulden, A.P. (1983), *De Meteorologische Aspecten van luchtverontreinigingsmodellen: Eindrapport van het Project Klimatologie Verspreidingsmodellen*, KNMI Scientific Report 83–4 (Royal Netherlands Meteorological Institute, De Bilt, The Netherlands).

Onderdelinden, D., van Jaarsveld, J.A., and van Egmond, N.D. (1984), *Bepaling van de Depositie van Zwavelverbindingen in Nederland (Determination of the Deposition of Sulfur Compounds in the Netherlands)*, Report 84217001 (National Institute of Public Health and Environmental Hygiene, RIVM, Bilthoven, Netherlands).

van Dop, H., Ridder, T.B., den Tonkelaar, J.F., and van Egmond, N.D. (1980), Sulfur dioxide measurements on the 213 m tower at Cabauw, the Netherlands, *Atmos. Environ.*, **14**, 933.

16. SUMMARY AND CONCLUSIONS OF MEETING

Joseph Alcamo* and Jerzy Bartnicki**
* *International Institute for Applied Systems Analysis, Austria*
** *Institute for Meteorology and Water Management, Poland*

16.1 ATMOSPHERIC MODEL UNCERTAINTY

A comprehensive procedure was presented to analyze LRT model uncertainty. The procedure was used to structure the uncertainty analysis of the EMEP-West long-range transport (LRT) model. Model uncertainties were organized into categories of *model structure, parameters, forcing functions, initial state*, and *model operation*. In applying uncertainty information to computations of total sulfur deposition in Europe, it was noted that a constant error range around the computed deposition yields greatly varying spatial and temporal patterns of sulfur deposition in Europe.

A general procedure was presented for using Monte Carlo simulation to analyze uncertainty due to parameters, meteorological inputs, and boundary and initial conditions. In a preliminary application the uncertainty in four parameters in the EMEP-West model was analyzed – dry deposition rate (v_d), mixing height (h), transformation rate (k_t), and wet deposition rate (k_w). The effect of these uncertain parameters on five state variables [SO_2 (air), SO_4^{2-} (air), dry sulfur deposition, wet sulfur deposition, and total sulfur deposition] was computed. The magnitude of computed uncertainty was different for the five state variables, with SO_2 (air) the largest and dry deposition the smallest. The influence of individual parameters on these state variables also substantially varied.

During the discussion it was noted that terminology connected with uncertainty analysis must be clarified, particularly the distinction between sensitivity analysis and uncertainty. *Model uncertainty* was defined as the "departure of model calculations from current or future 'true values'", but it was also pointed out that this definition is of limited use in practice. Instead, an indirect approach is taken to quantify uncertainty, for example by propagating uncertainties of model inputs through model equations, as in the aforementioned application of Monte Carlo simulation. In this case the frequency distribution of model inputs must be estimated by independent means. A problem of terminology arises, however, if all stochastic model inputs are

assigned, *a priori*, comparable frequency distributions. In this case results of the uncertainty analysis may be interpreted as a kind of sensitivity analysis.

Another paper focused on the variability of v_d over the sea. A theoretical model was presented which can be used to compute v_d based on the characteristics of air flow over water.

The variability of the local deposition parameter α in the EMEP-West model was studied using a combined Gaussian–*K*-theory model. The "equivalent" local deposition rate α' ranged from 0.0 for high emission sources and strong wind speeds to 0.76 for low sources, low wind speeds, and stable conditions. For intermediate source heights and meteorological conditions α' was computed to be near the EMEP-West value of $\alpha = 0.15$.

The uncertainty of computed sulfur deposition due to interannual meteorological variability was estimated by analyzing EMEP annual source–receptor matrices from 1978–1982. Annual average deviation of sulfur deposition in most grid elements was between 5% and 20%, with a typical deviation of 13%. This relatively low variability could be due to:

(1) Insensitivity of the EMEP model to meteorological variability.
(2) Actual meteorological variability not being large during 1978–1982.
(3) Natural compensation of sulfur sources and/or wind and precipitation.

A method was presented in another paper to take into account interannual meteorologic variability by creating a "climatologic-average" source–receptor matrix. This matrix could be created by relating monthly matrices to the frequency of occurrence of *Grosswetterlage* (GWL). The monthly matrices would be grouped to form an annual matrix such that the frequency of occurrence of GWL in this annual matrix is close to the long-term "climatologic normal" GWL frequency.

Another type of meteorologic uncertainty results from the possible consequences of long-term climate change on computed sulfur deposition. An empirical approach was introduced to contend with this uncertainty. The approach involves an analysis of the historical correlation between hemispheric temperature fluctuations and fluctuations in temperature and precipitation in various European subregions. This correlation could be the basis for estimating regional temperature and precipitation changes in Europe due to future scenarios of hemispheric temperature change.

16.2. STATUS OF LRT MODELS

It was reported that EMEP-West model output reasonably agrees with 58 months of data. Differences between output and data were attributed in part to measurement errors. A four-year average annual country-by-country sulfur budget was presented, which was thought to be a better long-term climatologic approximation than the previously available two-year budget.

Results from the EMEP-East model were also presented. The point was made that combining data collection and modeling was a more cost-effective way of computing transboundary pollutant flux than data collection alone. In a sample calculation, the atmospheric sulfur flux in a one-year period across an idealized CMEA boundary was 1.92×10^6 t sulfur in one direction and 1.42×10^6 t sulfur in the opposite direction.

Results from an NO_x long-range transport model were presented. The model contains very simple chemistry and a nonlinear parameterization of wet deposition. Model experiments indicated that the nonlinear wet deposition rate would result in a nonlinear source–receptor relationship between NO_x emission sources and nitrogen deposition receptors. However, it was found that halving the emissions had a smaller nonlinear effect than doubling the emissions.

In another paper a simple method was proposed to include oxidants in LRT model calculations. The method exploits the fact that the sum of NO_x and O_3 should be conserved in the atmosphere, even though they are individually reactive. Using a LRT model, the concentrations of NO_x, hydrocarbons, and total oxidant are first computed. Next O_3 is computed from its photostationary relationship with NO and NO_2.

16.3. INTERFACE BETWEEN ECOLOGICAL AND AIR QUALITY MODELS

In a paper presented from a forest ecologist's perspective it was noted that it would be desirable for regional scale forest impact models to have the following atmospheric inputs:

(1) For the temporal scale – annual average ambient concentrations with "relative" seasonal concentrations.
(2) For the spatial scale:
    (a) Within a tree stand, the ambient concentration above the canopy with "relative" vertical distribution within the canopy.
    (b) Between tree stands, dependence of ambient concentration on elevation.

In another paper, this time from an atmospheric scientist's perspective, it was pointed out that the spatial pattern of forest damage in the FRG can be better explained by the pattern of secondary pollutants, like O_3, than by the pattern of primary pollutants, such as SO_2 and NO_x. Moreover, pollutant flux might be even more relevant to forest damage than airborne pollutant concentration. For example, the sulfur flux to one remote station in FRG was a factor of 3–5 higher than that to an urban station.

It was reported that important linkages between atmospheric inputs and lake and soil acidification include "filtering" of pollutants by vegetation and deposition of acid buffering ions. A parameterization of the filtering process was proposed, which takes into account that sulfur deposition on forested land

has been measured to be a factor of 1.1 to 3.9 higher than on open land. In order to properly parameterize the deposition of base cations it is important to estimate whether this deposition will be additive or proportional to sulfur deposition.

In another paper the vertical distribution of airborne SO_2 was reported from a monitoring station in the Netherlands. The long-term average concentration at 4 m was found to be 0.74 times the concentration at 100 m when averaged over all stability classes. This ratio varied between stability classes. A theoretical model of the concentration profile in the surface layer based on similarity considerations yielded results close to observations.

16.4. RESEARCH RECOMMENDATIONS

(1) Uncertainty analysis as outlined in this Research Report depends on knowledge of frequency distributions of model inputs, such as parameters. Research should be devoted to improving estimates of these distributions.

(2) Trace gas measurements over the sea are needed to improve our understanding of pollutant long-range transport over the sea.

(3) In addition to the interannual variability of sulfur deposition, the variability of SO_2 air concentration should also be investigated.

(4) In order to link climate change and acidification, research must be conducted on how to convert information from climate change scenarios, i.e., precipitation and temperature changes over large time and space scales, into inputs suitable for LRT models.

(5) As noted in this Report, frequency analyses of *Grosswetterlagen* have potential applications in the evaluation of climate change impact on pollutant transport. Consequently, it is important to study the correlation between *Grosswetterlage* occurrence and meteorological variables, such as air temperature and precipitation.

(6) There is a need for an increased collaboration between atmospheric scientists and ecologists to improve our understanding of the interface between atmospheric phenomena and ecological impacts. The remaining recommendations pertain to this collaboration.

(7) From the point of view of ecological impact studies, it is important that LRT models take into account seasonal or shorter time-scale variability of pollutants.

(8) Detailed data of the vertical distribution of pollutants are needed so that layer-average LRT models can be linked to ecological impact models.

(9) More specifically, data are especially needed on:

   (a) The relationship between pollutant deposition onto open and forested land.

   (b) The deposition of cations capable of buffering the acidifying affect of sulfur deposition.

APPENDIX: MEETING PARTICIPANTS

Roel van Aalst	TNO, Delft, The Netherlands
Joseph Alcamo	International Institute for Applied Systems Analysis, Laxenburg, Austria
Jerzy Bartnicki	Institute for Meteorology and Water Management, Warsaw, Poland
Ruwin Berkowicz	Danish Air Pollution Laboratory, Copenhagen, Denmark
Karol Budzinski	Institute for Meteorology and Water Management, Warsaw, Poland
Anton Eliassen	Norwegian Meteorological Institute, Oslo, Norway
Gode Gravenhorst*	Alfred Wegener Institut für Polarforschung, Bremerhaven, FRG
Leen Hordijk*	International Institute for Applied Systems Analysis, Laxenburg, Austria
Sylvain Joffre	Finnish Meteorological Institute, Helsinki, Finland
Juha Kämäri	Finnish National Board of Waters, Helsinki, Finland
Annikki Mäkelä	International Institute for Applied Systems Analysis, Laxenburg, Austria
Janna Mikhailova	Institute of Applied Geophysics, Moscow, USSR
Göran Nordlund	Finnish Meteorological Institute, Helsinki, Finland
Maximilian Posch	International Institute for Applied Systems Analysis, Laxenburg, Austria
Sergei Pitovranov	International Institute for Applied Systems Analysis, Laxenburg, Austria
Jerzy Pruchnicki	Institute for Meteorology and Water Management, Warsaw, Poland
Eliodoro Runca*	Technital, Verona, Italy
Jørgen Saltbones	Norwegian Meteorological Institute, Oslo, Norway
Joop den Tonkelaar	Royal Netherlands Meteorological Institute, de Bilt, The Netherlands
Ted Turner	Atmospheric Environment Service, Toronto, Canada

* Session Chair